

Lowest-Energy Crystalline Polymorphs of P3HT

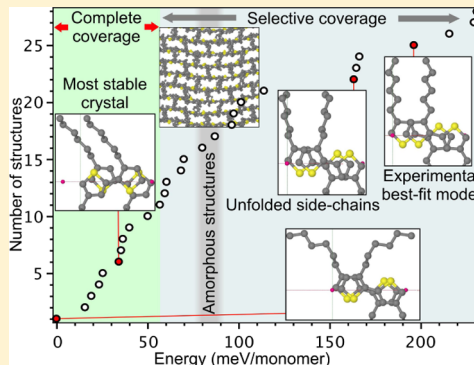
Andriy Zhugayevych,^{*,†,ID} Olga Mazaleva,[†] Artem Naumov,[†] and Sergei Tretiak^{*,†,‡,ID}

[†]Skolkovo Institute of Science and Technology, Moscow 143026, Russia

[‡]Theoretical Division and Center for Integrated Nanotechnologies, Los Alamos National Laboratory, Los Alamos, New Mexico 87545, United States

Supporting Information

ABSTRACT: We systematically study low-energy crystalline polymorphs of the archetypal conjugated polymer, regioregular poly-3-hexylthiophene (rr-P3HT) using the best available density functional theory methods benchmarked against the ab initio coupled cluster method. A comprehensive conformational search is performed for two-dimensional π -stacks being the most rigid structural unit of bulk P3HT. We have identified a number of nearly isoenergetic polymorphs below the energy level of room-temperature amorphous structures and well below the energy of optimized best-fit experimental models. Classical molecular dynamics simulations show that these crystals retain their structure at least at 200 K. At room temperature, although the conjugated backbone of the π -stack remains ordered, aliphatic side chains are melted, transforming from low-energy folded conformations to high-entropy fully unfolded structures. Our study shows that P3HT is a statistically frustrated system with multiple competing interactions, which complicates fabrication of highly ordered bulk forms but gives structural flexibility of glasses.



INTRODUCTION

Poly-3-hexylthiophene (P3HT) is a workhorse of modern organic electronics. Despite a modest intrinsic performance, owing mostly to high bandgap and relatively low hole mobility, the highly developed processing protocols of this material make it commonly usable in various prototype devices as well as in basic research seeking structure–property relationships. Numerous studies have provided a detailed understanding of P3HT structure at various scales down to atomic resolution.^{1–4} Yet at the smallest scale, the atomistic structure of P3HT evades a complete resolution because of substantial intrinsic disorder and related fundamental challenges in growing perfectly ordered crystals.^{5,6} In particular, little is known about low-energy polymorphs of a crystalline regioregular P3HT (rr-P3HT). Here, the regioregularity means ordered attachment of alkyl chains along the polymer, see Figure 1, which is essential for constructing an ideal crystal. Although the mesoscale structure of a material may be unsusceptible to subtle microscopic variations, electronic properties are sensitive to small changes in intrachain and intermolecular packings,⁷ requiring accurate knowledge of atomic positions. A recent discovery of two electronically different coexisting aggregates of P3HT⁸ is an example of such phenomena.

The mesoscopic structure of P3HT material is determined by several levels of packing, as shown in Figure 1. The smallest building block is the π -stack of individual polymer chains. It is relatively rigid due to covalent bonds along the chain and strong (by contact area) noncovalent bonding between the chains. These two-dimensional layers are packed into a bulk solid by noncovalent interactions between side chains. In most

of the observed P3HT morphologies, side chains are not interdigitated, which is referred to as type-1 packing (form I). The resulting three-dimensional structure can grow along the two “noncovalent” directions: π -stacking and side-chain contacts, thus forming tiles (lamellae in polymer physics⁹), whose principal facets are terminated by broken or folded polymer chains referred to as ties. Finally, the lamellar packing of such tiles determine the mesoscopic structure of P3HT.¹ Other nanoscale morphologies exist, including aggregates⁸ and epitaxial layers,¹ which may have different mesoscale ordering, whereas the π -stacking seems to be the common structural motif for most of the known forms of P3HT. Another argument to consider π -stack as a fundamental building block of P3HT stems from the electronic structure: strong electronic couplings between monomers inside the π -stack form a continuous two-dimensional network, whereas couplings between π -stacks are negligible¹⁰ except for incoherent Förster energy transfer through space or charge carrier hopping through tie chains.

To resolve P3HT structure at the smallest scale, many structural studies by different techniques have been conducted, including electron diffraction,¹¹ X-ray diffraction augmented with NMR crystallography,¹² cryotransmission electron microscopy,³ and other methods.^{6,13} These experiments typically directly measure only unit cell parameters, whereas atomic positions are estimated by best-fit modeling.^{5,11,12} Indirect

Received: November 14, 2017

Revised: March 27, 2018

Published: March 29, 2018

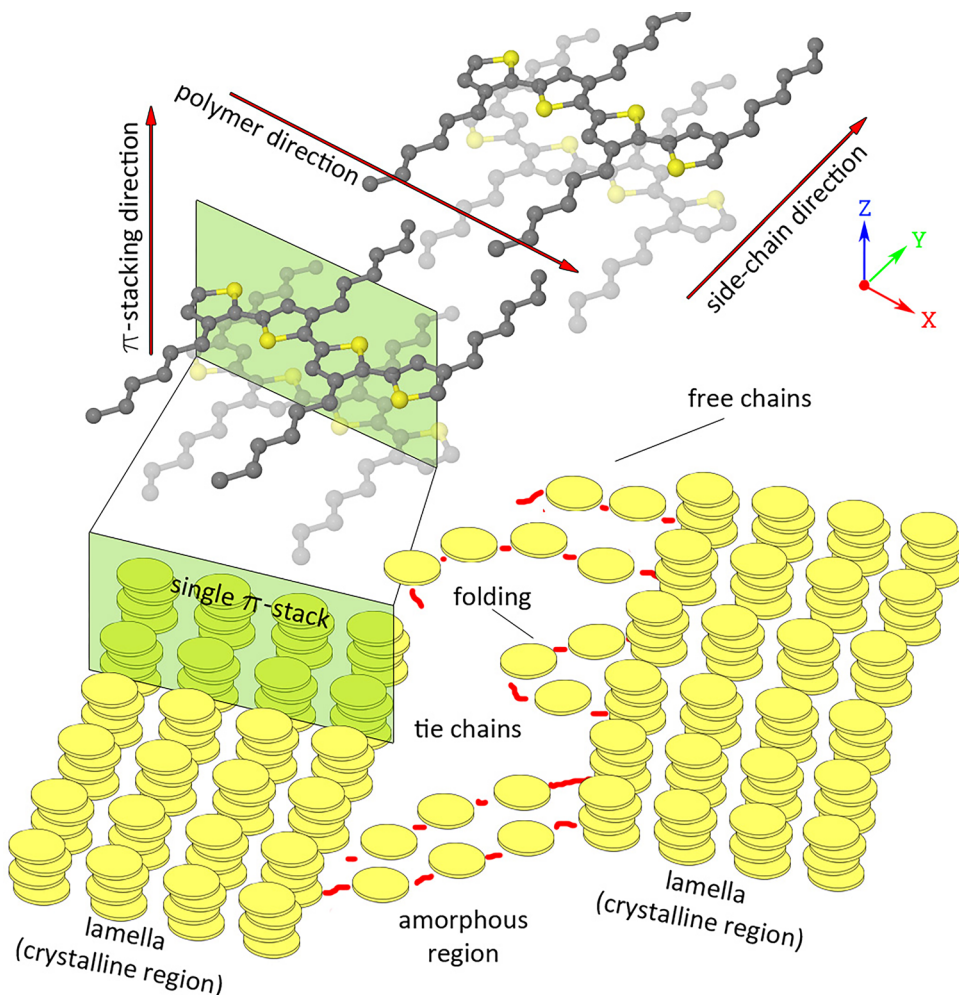


Figure 1. P3HT structure with four levels of packing: polymer, π -stack, interstack packing by side-chains into lamellae, and lamellar packing.

methods, such as inelastic neutron spectroscopy,⁵ Raman spectroscopy,¹⁴ and solid-state nuclear magnetic resonance,⁶ provide useful restrictions on possible atomic arrangements, but they still require an a priori predicted set of structures. Available experimental data suggest a monoclinic cell with the space group $P2_1/c$.^{6,11} Reported cell parameters vary within several percents; see Table 1. The value of the monoclinic angle is somewhat uncertain, but all recently reported values deviate from the right angle by less than 6° , which is the angle obtained by shifting adjacent π -stacks by half of the $\pi-\pi$ distance. This is consistent with absence of specific interactions between π -stacks in type-1 packing (no strong correlations between intra- and inter- π -stack orders). Instead, the stacks pack as textured bricks. Values of other geometric parameters, such as the setting angle and side-chain dihedrals, vary substantially from report to report, e.g., the setting angle is almost 0 in ref 12 and is about 30° in ref 11. In addition, it is unclear if the reported atomic positions correspond to a minimum of potential energy surface (PES) or to an ensemble average of multiple local arrangements.^{6,15} This concerns side-chain conformations, setting angle, and interpolymer packing. In particular, it is unclear if regioregular polymer chains are π -stacked regularly (all reported unit cells have antiparallel stacking) or have random forward–backward orientation.

Reported systematic computational studies of semicrystalline P3HT are mostly based on classical molecular dynamics

(MD).^{22–26} Although yet to be able to sample the entire conformational space of bulk P3HT, existing density functional theory (DFT) calculations generally converge to a few polymorphs of interest.^{5,27,28} All such recent investigations focus on the same structural motif consistent with available experimental results. At the same time, no consensus has been achieved on atomic positions within the unit cell, neither is there a common parameterization of the P3HT geometry to differentiate and categorize that zoo of structures available in the literature. It seems natural for polymers that the origin of such diversity is a pronounced polymorphism, so that local atomic arrangements are sensitive to variations in processing conditions or computational methods.²² Several force field parameterizations have been developed for P3HT using DFT calculations of intramolecular blocks, such as dihedrals and atomic charges, giving reasonable geometry compared to available experimental data.^{23,29–33} Yet the main concern of classical force fields is accuracy: although most of the structural features observable experimentally at elevated temperatures are well reproduced in modern simulations, the accuracy of atomic positions is uncertain without reliable validation by experimental or ab initio data, both of which are too scarce today.

Thus, after decades of experimental and theoretical study of P3HT, we are still lacking precise knowledge of its possible microstructures at the scale of individual atom positions in bulk material. Motivated by this need, here we perform a systematic

Table 1. Recently Reported Parameters of P3HT Unit Cell (in Chronological Order) Along with Relevant Results from the Present Work^a

method	polymer (Å)	π-stack (Å)	side-chain (Å)	angle (deg)
Type-1 Structures				
X-ray + AFM ¹⁶	7.7	7.7	16.8	90
X-ray, str. 1 ¹⁷	7.6	7.8	17.2	105*
X-ray, str. 2 ¹⁷	7.6	7.7	16.9	100.7*
X-ray ¹⁸	7.7	7.7	15.7	87
ED ¹¹	7.8	7.8	16.0	86.4
X-ray + NMR ¹²	7.7	7.6	16.4	87
cryo-TEM ³		7.6	17	
X-ray + ED ¹⁹	7.6	7.8	16.7	85
str. ¹² at 300 K	7.68	8.2	16.0	95.0
str. ¹² by OPLS	7.78	7.1	18.3	94.5
str. ¹² by PBE-MBD	7.79	7.1	17.9	88.9
str. ¹² by vdW-DF2	7.86	7.4	17.2	86.5
Interdigitated (Type-2) Structure				
ED, str. P3HT-26 ²⁰		9.3	13.1	68.5
X-ray ²¹		8.8	12.0	
this work (OPLS)	7.81	8.7	13.2	70.2
this work (PBE-MBD)	7.80	8.9	13.3	69.9
this work (vdW-DF2)	7.89	9.1	13.5	69.3

^aThe three translation vectors are labeled as follows: “polymer” means direction along the polymer; the angle is between “π-stack” and “side-chain” axes except for the two values labeled by asterisk where the angle is between polymer and side-chain axes. The “str.¹²” is the crystal structure reported in ref 12. The unit cell “at 300 K” is simulated by molecular dynamics (MD); the other calculated structures are optimized by the indicated method.

DFT-based scan of a low-energy high-symmetry region of conformational space of bulk rr-P3HT to resolve the uncertainties discussed above and to provide reference data for follow-up studies by improved force fields and multiscale modeling. We start with benchmarking best available DFT methods using high-level theory and experimental crystal data for P3HT and its fragments. Then, we develop a coarse-grained model of P3HT, allowing for efficient parameterization of various crystalline polymorphs as well as for recognition of local structural patterns in amorphous phases. Using the developed methodology, we search for low-energy polymorphs of rr-P3HT, targeting a complete coverage below the energy level of known room-temperature polymorphs and, in addition, within the energy basins of all experiment-derived atomistic models.^{11,12,20} After comprehensive sampling of P3HT microstructures, we analyze them to understand common structural motifs of rr-P3HT. Also, we address specific questions related to possible interpretations of best-fit models, use of vibrational spectra to distinguish polymorphs, and understanding of glass forming properties of rr-P3HT, including transition from low-energy to room-temperature structures.

■ COMPUTATIONAL METHODOLOGY

To get accurate description of bulk P3HT at a relevant spatial scale, we apply a combination of three approaches: ab initio coupled cluster method, DFT, and classical force field. As the reference method, we use explicitly correlated local coupled cluster theory with single, double, and perturbative triple excitations DF-LCCSD(T)-F12,³⁴ as implemented in MOLPRO program.^{35,36} The computations are performed with the cc-pVTZ^{37,38} orbital basis set and cc-pVTZ/MP2fit and cc-

pVTZ/JKfit basis sets for density fitting. We refer to this method as CCSD(T)/cc-pVTZ.

The main results of this work are obtained at the DFT level. Here, proper choice of the density functional is critical.^{39,40} Consequently, a preselected set of functionals is benchmarked against CCSD(T) using representative fragments of P3HT, including its monomer and oligomers of polyethylene and polythiophene, with emphasis on noncovalent interactions and π-conjugated dihedrals. We assess several density functionals commonly applied to π-conjugated molecules: B3LYP, CAM-B3LYP, LC-ωPBE, and ωB97X.^{39–41} Noncovalent interactions are of primary importance for P3HT structure; therefore, dispersion corrections are added to these DFT models.⁴² We use the D3 correction with Becke–Johnson damping,⁴³ except for ωB97X, which is considered in ωB97XD version.⁴⁴ In the selection of a basis set, we use the minimalist approach to be able to efficiently model bulk P3HT. We test several Pople’s basis sets ranging from the minimally acceptable 6-31G*^{39,45} up to 6-311+G(3df,2p). All molecular DFT calculations are performed using Gaussian 09 program.⁴⁶ To simulate bulk P3HT in a super cell, we need to apply periodic boundary conditions, which are not implemented for the dispersion-corrected functionals in Gaussian 09. For this type of calculation, we use the plane-wave basis with two methods: vdW-DF2^{47,48} and many-body dispersion (MBD)-rsSCS,⁴⁹ referred here as Perdew–Burke–Ernzerhof (PBE)-MBD. The former method is based on nonlocal correlation functional, accounting for van der Waals interactions with rPW86^{50,51} exchange term. It was shown to be accurate in predicting the structure of organic crystals.^{52–54} PBE-MBD represents another way for accounting dispersion interactions using PBE⁵⁵ density functional coupled with many-body Tkatchenko–Scheffler van der Waals model. It employs range separation of the self-consistent screening of polarizabilities so that the long-range correlation energy can be separated from the short-range functional contribution. Calculations with the plane-wave basis are performed in VASP 5.4 program.⁵⁶ More specifically, we use VASP-default PAW pseudopotentials⁵⁷ and 600 eV energy cutoff. Γ-Centered Monkhorst–Pack grid with at least 30 k-points per Å⁻¹ is fixed for all polymorphs under comparison. Geometry optimization is performed with tight criteria predefined in both Gaussian and VASP programs. In VASP maximum gradients typically do not exceed 20 meV/Å for PBE-MBD and 10 meV/Å for vdW-DF2. Unit cells are optimized using fourth-order polynomial fit of energy for a set of fixed-volume relaxations.

The results of assessment of density functionals are summarized in Table 2 (see the Supporting Information for comprehensive analysis). For polyethylene, we calculate difference in energies of all-trans and hairpin conformers of short oligomers with the reference CCSD(T) energies taken from ref 58. For polythiophene tetramer, we compare energies of several conformations sampling inter-ring dihedrals relative to the planar one. Finally, for P3HT monomer, we consider a set of low-energy conformers. According to Table 2, CAM-B3LYP-D3 is the most accurate density functional for the considered datasets, having deviations from the reference calculations well below the “chemical accuracy” level of 1 kcal/mol ≈ 43 meV. The basis set 6-311G* seems to provide a good trade-off between accuracy and numerical efficiency, having only several millielectronvolts difference from 6-311+G(3df,2p), which is substantially smaller than variations of conformer energies upon change of density functional. For

Table 2. Assessment of Density Functionals for P3HT Fragments: Polyethylene (PE), Polythiophene (PT), and P3HT Monomer (M)^a

dataset size	PE	PT	M
	6	7	72
Fixed Basis Set 6-311G*			
CAM-B3LYP-D3	5	9	5
B3LYP-D3	16	5	12
PBE-MBD	22	23	13
vdW-DF2	19	20	17
LC- ω PBE-D3	50	15	24
ω B97XD	90	16	26
OPLS	118	54	56
CAM-B3LYP	195	9	64
Fixed Functional CAM-B3LYP-D3			
6-311G*	5	9	5
6-311G**	8	8	6
6-311+G(3df,2p)	10	1	12
6-31G*	19	6	6

^aThe entries are the root mean square deviation for conformational energies (relative to the lowest-energy conformer) with respect to the reference CCSD(T)/cc-pVTZ values. All energies are in millielectronvolts. The geometry is fixed at MP2/cc-pVTZ for polyethylene and at CAM-B3LYP-D3/6-311G* for other systems. The details are given in the main text, Table S4, Figure S10, Table S6.

plane-wave basis, both PBE-MBD and vdW-DF2 methods show accuracy comparable with the best hybrid functionals. The former gives slightly better energies and geometries for P3HT monomer (see Table S7), whereas the latter is computationally more efficient for bulk solids. In addition, we have performed geometry comparison for relevant crystals with fully resolved atomic positions: polyethylene,⁵⁹ quarterthiophene,⁶⁰ and type-2 P3HT,²⁰ showing the same trend, see Table S8. Consequently, CAM-B3LYP-D3/6-311G*, PBE-MBD, and vdW-DF2 are the three methods used for all subsequent DFT calculations performed in this work. When the results are essentially the same for all three functionals, we use the word “DFT” without specifying a specific functional.

Classical force field simulations are used to obtain the initial guess for geometry of possible P3HT polymorphs as well as to investigate dynamic and kinetic stability of the obtained structures. We use LAMMPS program⁶¹ and optimized potentials for liquid simulations (OPLS)-style^{62,63} force field. The parameters are taken from ref 30 with two modifications: we neglect the fifth order coefficient for the inter-ring dihedral and use long-range electrostatics to avoid artifacts in geometry optimization. Comparison with experimental geometries of crystals of oligomers³⁰ and DFT-optimized geometries obtained in the present work shows that this OPLS force field gives accurate geometries. However, the total energies are inaccurate with the standard deviation exceeding 40 meV/monomer (1 kcal/mol, see Figure S27). MD simulations are performed in NPT ensemble at zero pressure with the artificial periodic dimensions (two for polymer, one for π -stack) uncoupled from barostat. The time step is 1 fs. Geometry relaxation is performed by alternation of conjugated gradients and damped dynamics (“fire” style⁶⁴) to overcome shallow traps on PES.

METHODOLOGY FOR STRUCTURAL SEARCH AND ANALYSIS

To describe the structure of bulk P3HT quantitatively, we coarse-grain it by replacing each monomer by a reduced set of parameters fully characterizing the monomer geometry up to nonessential fluctuations; see Figure 2. This set includes: three

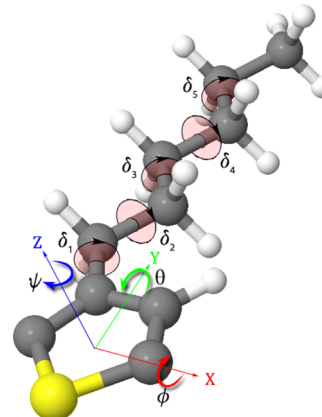


Figure 2. Coarse-grained coordinates of a single P3HT unit: three translations (x, y, z), three rotations (ϕ, θ, ψ), and five dihedrals ($\delta_1 \equiv \delta, \delta_2, \dots, \delta_5$).

Cartesian coordinates (x, y, z) of the center of the thiophene ring, three Euler's angles (ϕ, θ, ψ) rotating the thiophene ring from a canonical orientation to the actual one, and five dihedrals ($\delta_1, \dots, \delta_5$) defining conformation of the side chain. This parameterization reduces the coordinate space from 25×3 correlated Cartesian coordinates per monomer to 11 nearly independent parameters. Only three of them show nontrivial dynamics at room temperature: x, ϕ , and $\delta \equiv \delta_1$. The other eight coordinates include four low-amplitude motions along y, z, θ , and ψ and four quasi-discrete variables $\delta_{2\dots 5}$. Instead of listing values of these coordinates, it is more convenient to encode all possible combinations of them up to nonessential fluctuations. In particular, all side-chain conformations are fully described by five lowercase letters. Each letter encodes a value of a side-chain dihedral: *a* (180°), *b* (-60°), and *c* ($+60^\circ$). The dihedral δ is special: we use *a* for $\delta > 0$ and *b* for $\delta < 0$ provided that the dihedral is counted from the bridging carbon. Although there are five dihedrals to encode, we omit trailing *a*-s to avoid long notations; e.g., *aacaa* is cut to *aac* when encoding a side chain with $\delta_1 > 0$, $\delta_3 \approx 60^\circ$, and $\delta_{2,4,5} \approx 180^\circ$. These notations are exemplified in Figure 3. Rigorous definition of all parameters and complete encoding of a monomer are given in Section S1.

To encode a crystal structure with a monomer being the asymmetric unit, we combine the above defined side-chain code of the monomer (lowercase letters) with a code describing orientation of thiophene rings in the unit cell (uppercase letters). For 2×2 cell, 16 different structural arrangements of the 4 thiophene rings can be identified (see Table S2) and labeled by 2 capital letters, as shown in Figure 4. In addition, there are two special fully planar cases denoted as *C* and *B*. In summary, any rr-P3HT crystal with 2×2 unit cell can be labeled by a string of up to two uppercase letters denoting lattice structural type and up to five lowercase letters encoding conformation of the side chain of the asymmetric unit, e.g., *CBaac* (see Figure S23 for illustration). Importantly, any two low-energy crystals with the same code have nearly the same

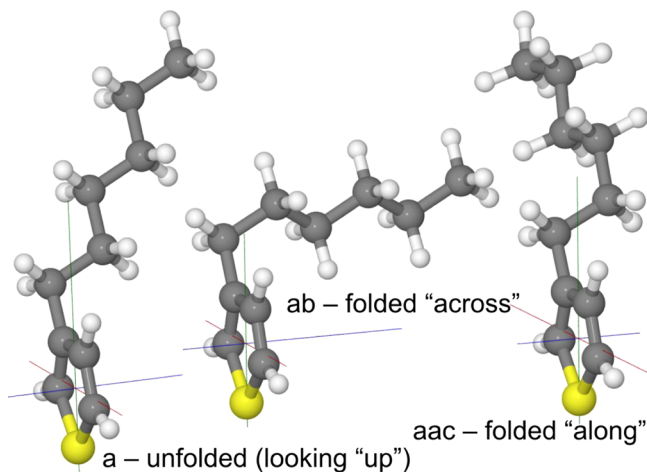


Figure 3. Three conformers dominating in low-energy (*aac*, *ab*) and high-entropy (*a*) structures. Conformer *a* has all dihedrals at their optimal values: $\delta_1 \equiv \delta \sim 110^\circ$ and $\delta_{2..5} \approx 180^\circ$ so that the side chain is directed out of the π -stack plane. Conformer *ab* differs only by $\delta_2 \approx -60^\circ$, resulting in side chain oriented perpendicular to the thiophene ring. Conformer *aac* has $\delta_3 \approx 60^\circ$, and the side chain is directed along the polymer chain.

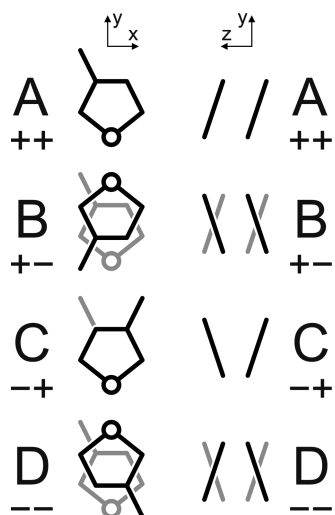


Figure 4. Structural type notations for a 2×2 cell. Two signs on the left encode orientation of the foreground polymer relative to the background one in xy -plane: forward-backward (sign 1) and up-down (sign 2). Two signs on the right encode orientation of the setting angle for adjacent monomers: coplanar-anticoplanar (sign 3) and eclipsing-staggered (sign 4). For convenience, each pair of signs is encoded by a letter from A to D. Note that only the sign 1 is topological for the molecular dynamics considered in this work (parallel or antiparallel stacking). For illustration, see examples of structural types in Figures S22–S26.

structure, differing mainly by parameters corresponding to large amplitude motions, x , φ , and δ .

Predicting the structure of bulk polymers and molecular solids is a challenging problem.^{9,54,65} There are two basic approaches: enumerative search⁶⁶ and simulation of experimental synthesis and processing.^{23,67} The latter approach should give more realistic geometries for each particular experiment, whereas the former one allows for a systematic itemization of all structures possible under a given search constraint. For this reason, we use a combination of both approaches, applying them alternately. We limit our search

space to experimentally observed structural motifs, which can be reduced to a four-monomer unit cell (2×2). In fact, it is the smallest reasonable cell for P3HT. Indeed, the polythiophene backbone prefers the trans-conformation, setting the minimum period along the polymer chain to two monomers. Commonly assumed polymer reversal symmetry requires that adjacent chains in the π -stack go in the opposite directions (antiparallel stacking), setting the minimum period along the π -stack to two chains. The initial iteration of the search algorithm includes only high-symmetry configurations. Further, we expand the search space by running MD starting from already identified crystalline polymorphs. By high-symmetry we mean a cell with the minimum asymmetric unit, which is a single monomer. Under such constraints, all possible layer symmetry groups are listed in Table S2. The precise algorithm for structural search is detailed in Section S2.

RESULTS AND DISCUSSION

Conformational Preferences of P3HT Fragments. We start our analysis with discussion of conformational preferences of small P3HT fragments to understand basic interatomic interactions determining structure of bulk P3HT. All possible conformers of the side chain can be readily enumerated using hydrogen passivated P3HT monomer. In a polyethylene, each C–C–C–C dihedral alone prefers trans-conformation. The two gauche conformers are low enough in energy, 20 meV, to be important for room-temperature structure of P3HT. In addition, the rotational barrier is only 125 meV, imposing no kinetic constraints for thermal equilibration of the entire PES of side-chain dihedrals.⁶⁸ Steric constraints may limit fluctuations of the dihedrals located close to the polymer backbone, such as δ_2 , whereas the terminal dihedrals, such as δ_5 , are flexible in type-1 interstack packing. The PES for δ_1 is more shallow (Figure S12), with the global minimum at 107° . Yet the cost of planarization is about 65 meV, which is high enough to keep nonplanar conformation also in bulk P3HT, although with substantial spread in values of δ_1 from ~ 90 to 180° (Table S11). By taking into account nonbonded interactions, we find their energy sufficient enough to substantially influence conformational preferences. Indeed, in bulk polyethylene the interchain interaction energy is 25–50 meV per carbon (Table S5). As a result, several conformers have their energy smaller or similar to that of the fully unfolded *a*-conformer,⁶⁹ which is prevalent in room-temperature crystals. The lowest-energy conformation is *ab* ($\delta_2 \approx -63^\circ$), smaller by 18 meV relative to *a*-conformer. Noticeably, both experimentally derived models of P3HT^{11,12} suggest an almost linear side chain, with the only twist at $\delta_2 \approx -133^\circ$. Such value corresponds to a saddle point on PES, and full relaxation of these models as isolated π -stacks by OPLS force field yields *a*-conformer for ref 12 and *ab* conformer for ref 11. Overall, a variety of low-energy conformers for a single monomer should result in combinatorially rich conformational space of bulk P3HT, whereas shallow barriers make these conformers dynamically accessible on a nanosecond scale.

The other nonvibrational intramolecular degree of freedom is the inter-ring dihedral. The geometry of the bithiophene is nonplanar by $\sim 30^\circ$ in both trans and cis conformations, in agreement with the experiment⁷⁰ (see PES in Figure S8). However, the planarization energy is only 10 meV and is decreasing with the oligomer size, so that thermal fluctuations and nonbonding interactions in bulk P3HT result in a broad distribution of the inter-ring dihedral. Overall, the geometry of

the isolated P3HT polymer is far from being highly symmetric and there is a multitude of close in energy conformations, which should influence intermolecular packing.

Bulk Crystals. To discuss bulk systems, it is important to understand partitioning of their binding energy. Organic molecular crystals show clear separation of various interatomic interactions by strength, concomitant to different levels of structuring.⁷¹ This includes strong covalent bonds forming a molecular framework, weaker intermolecular forces forming a π -stacking order, even weaker undirectional forces connecting π -stacks in a bulk material, and variable-strength noncovalent intramolecular interactions shaping individual molecules.⁷² The same picture is expected for P3HT. Indeed, the π -stacking energy is 0.4 eV/monomer for parallel stacking (structure *B*) and 0.5 eV for the antiparallel one (structure *C*). This means that the π -stack is a strongly bound system, although slips along the polymer direction are possible at elevated temperatures.⁶ The interstack interaction energy in the reported crystalline geometry¹² optimized by DFT is about 0.1 eV/monomer. In type-1 packing, this energy is distributed among multiple side-chain ends coming in and out of contact upon thermal fluctuations, in contrast to π -stacking energy concentrated in between each pair of polymers constantly. Therefore, the role of interstack interaction in formation of a structural order within π -stacks is small. Indeed, the relaxed geometries of the reported crystal¹² and its isolated π -stack counterpart differ insignificantly; see Table S11. Also, even at 100 K, MD snapshots of isolated π -stacks and crystals show essentially the same intrastack topology (compare Figures S17 and S16). Consequently, a type-1 P3HT crystal can be considered as a system of weakly interacting π -stacks.

Comparison of experimental and calculated geometries for bulk crystals is given in Table 1 (unit cell parameters) and Table S9 (coarse-grained coordinates). Type-2 crystal has no intrinsic disorder because DFT-optimized structure agrees well with the experimental one. There is some discrepancy in x and δ_2 parameters, but upon structural relaxation, the experimental best-fit model²⁰ readily converges to the DFT-predicted geometry. Type-1 crystals are different, at least for experiments with published atomic positions.^{11,12} Both DFT and OPLS force field relaxations of the geometry from ref 12 end up with the optimized structure very similar to the original one, see Table 1. The geometry from ref 11 contains crowded atoms, preventing DFT relaxation, but its formal optimization by OPLS results in the same structure as the one obtained from ref 12. Importantly, experimentally observed cell parameters are much closer to room temperature MD values than to the relaxed geometries, implying that the reported experimental geometries correspond to some average coordinates rather than to a local minimum. Also, the total energy of the DFT-optimized published type-1 crystal is significantly higher than the energy of several polymorphs of isolated π -stack; see e.g., Table S11. Therefore, in the observed type-1 crystals, a substantial intrinsic disorder is present and thus it is natural to expect a pronounced polymorphism for type-1 P3HT.

Polymorphism of π -Stacks at Zero Temperature. On the basis of the search methodology and energy distribution of generated structures (Figure S19), we expect a comprehensive coverage (by force field) of high-symmetry π -stacks within the energy of 150 meV/monomer, as counted from the lowest-energy polymorph. Because the standard deviation of the OPLS energy relative to DFT values is about 50 meV (Figure S27), we expect accurate identification of the lowest-energy

polymorphs by DFT within 50 meV range and representative coverage of unfolded conformers up to 200 meV (Table S11). The detailed list of polymorphs is given in the Supporting Information: Table S10 for the OPLS force field, Table S11 for PBE-MBD, and Table S12 for vdW-DF2. A short summary is presented in Table 3 with selected structures illustrated in Figure 5.

Table 3. List of the Lowest-Energy π -Stacks Categorized by Parallel/Antiparallel Stacking and Side-Chain Conformation: Unfolded *a*, Packed Along Polymer *aac*, and Along π -Stacking *ab*^a

		<i>a</i>	<i>ab</i>		<i>aac</i>	
Antiparallel	<i>C</i>	95	CA	17	CA	0
	CA'	145	CB	54	CB	13
Parallel	<i>BD</i>	45	BA	15	BA	44
	<i>BB</i>	79	<i>BD</i>	55	<i>BB</i>	48

^aPBE-MBD energies are given in milli electronvolts per monomer relative to the minimum energy of a π -stack (polymorph CAaac). CA' is the optimized π -stack from ref 12. See the complete list in Table S11.

Analysis of low-energy polymorphs (Table S11) shows two dominating side-chain conformations: *aac* and *ab*; see Figure 3 and Table 3. Both have a tightly packed structure: *aac* with side chains parallel to the polymer and *ab* with side chains perpendicular to the polymer (*abab* at 45 meV is a variation of the latter). Entropically stable unfolded conformers (*a* and *b*) start to appear at much higher energies of 80 meV, except for *BDa* structure at 45 meV, whose exceptional stability will be discussed later. In particular, one of the lowest-energy unfolded polymorphs of antiparallel stacking is the structure with the maximum possible symmetry, structure *C* at 95 meV. This geometry allows for tight packing of unfolded side chains, similar to what is achieved in *BDa* polymorph for parallel polymers. In the experimentally reported crystal,¹² packing of side chains is different so that each of them interacts with four side chains from the adjacent π -stack (C–C distances are 4.0 ± 0.1 Å). Overall, the three conformations *a*, *ab*, and *aac* dominate low-energy polymorphs up to 150 meV (Figure S20). Distribution of lattice types is more uniform, suggesting a relative flexibility of inter-ring dihedrals and π -stacking of thiophene rings, in agreement with the recently proposed model.⁶ Steric constraints suppress the *xy*-arrangements A/D and *zy*-arrangements C/D in Figure 4 so that (B/C)(A/B) combinations prevail (Table 3).

Lifting symmetry restrictions of Table S2 neither leads to principally new structures nor changes the overall energy landscape, except for amorphous structures discussed later. Typical symmetry breaking results in modulation of monomer parameters either along the polymer chain or along the π -stacking. Such modulations often lower the energy for the OPLS force field, whereas DFT calculations show that a more symmetric structure is usually more stable, consistent with 2 × 2 unit cell symmetry with the smallest asymmetric unit. Another symmetry readily broken in isolated π -stacks is the symmetry of their two facets ($y > 0$ and $y < 0$) because the side chains attached to the opposite facets do not interact directly with each other. Comprehensive investigation of possible low-symmetry polymorphs is limited by accuracy of the force field.

The translation period of the polymer is 7.80(2) Å for all DFT-optimized polymorphs, implying that the experimentally

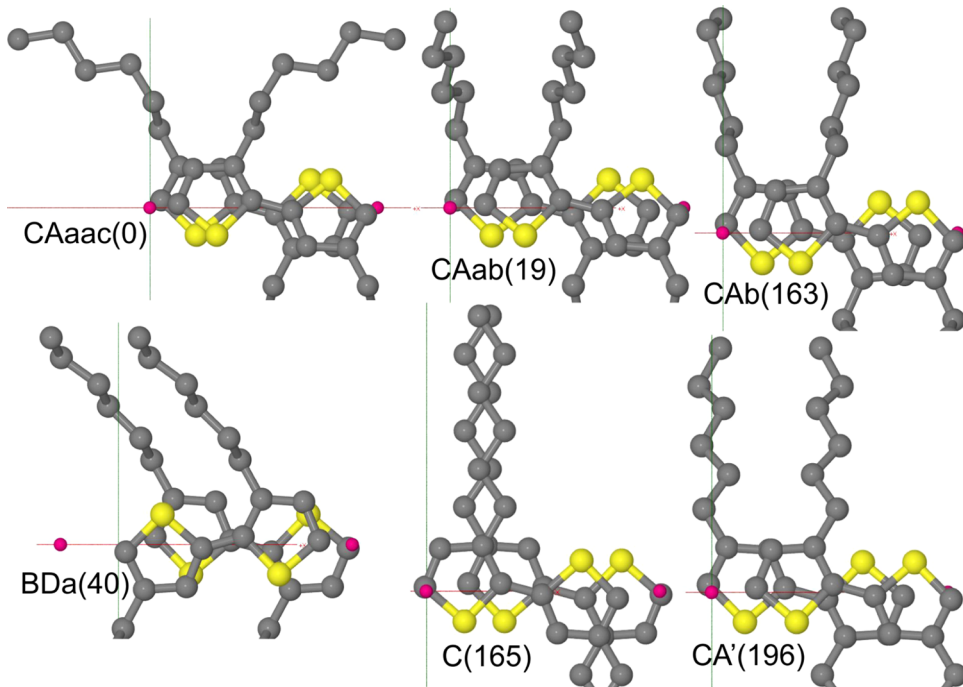


Figure 5. Unit cells of selected polymorphs viewed along z -axis. The vDW-DF2 energies in milli electronvolts are given in parentheses. Unit cells are denoted by translation vectors starting at the origin and ending at magenta balls. The x - and y -axes are marked by red and green colors, respectively.

observed shrinkage to 7.6 Å is caused by thermal disorder. Most of the calculated values of the π -stack period vary from 7.4 to 7.9 Å in consistency with experiments. Extra large values (>8 Å) correspond to large setting angles ($>30^\circ$), and might contribute to a quenched disorder in bulk P3HT. The dihedral δ for most of polymorphs deviates from the optimal single-molecule value by no more than 20° , corresponding to rather small penalty of about 10 meV. Exceptions from this rule are rare and include the two highest-symmetry structures C and B , and experimentally derived geometry, even though a bias toward optimal values of dihedrals has been set by the search algorithm. In any case, substantial deviation between experimental and computed geometries of type-1 crystal as well as existence of a number of polymorphs energetically and structurally similar to the experimental one, support the idea that the observed structure is an averaged one, and a multitude of geometrically distinct isoenergetic microstructures may coexist both dynamically due to thermal fluctuations and as a quenched disorder.

Elevated Temperatures. Our present study of P3HT at nonzero temperatures is limited by accuracy of the available force field so that the results should be considered only qualitatively: we are not predicting room-temperature structure but rather investigate how given low-energy polymorphs are transforming at elevated temperatures, to derive generic conclusions applicable for DFT structures as well. Again, type-1 and type-2 crystals behave differently. Type-2 crystal is the lowest-energy polymorph among all known bulk P3HT forms, being more stable than the lowest-energy π -stack by 128 meV/monomer. It is thermally stable at room temperatures under periodic boundary conditions (Figure S18), consistent with the experimentally measured melting temperature of 400 K for long oligomers.²¹ In contrast, type-1 crystals and isolated π -stacks undergo order-disorder transition at some temperature below 300 K; see Table S10. For π -stacks, after 1 ns MD at 400 K followed by 1 ns quench, all studied crystalline

polymorphs transform into one of four structures identified as $a-CBa$, $a-Ca$, BDa , and $a-Ba$, as shown in Figure S16. Here, “ a ” means amorphous and $a-Ca$ means that polymer chains are ordered in the xy -plane and disordered in the yz -plane (see Figure 4). The dihedral δ_1 is also ordered, whereas the rest of degrees of freedom are disordered within the used 2×2 unit cell identification algorithm. This means that at elevated temperatures, side chains melt (except for δ_1), setting angles fluctuate, and polymer chains can slip along x -direction. As a result, at room temperature, type-1 semicrystalline rr-P3HT is substantially disordered. An exception is BDa polymorph which might preserve its crystalline order at elevated temperatures (the available force field shows no melting even at room temperature). Interestingly, we observe two polymorphs per topological class (parallel/antiparallel stacking). They differ by their setting angle pattern: ordered for $a-CBa/BDa$ and disordered for $a-Ca/Ba$ (see Table S10). This result is consistent with the hypothesis of ref 8 that the two optically distinct P3HT phases have similar electronic structure and vibronic couplings but shifted exciton levels due to disorder effects.

Although probing dynamics with DFT is not computationally efficient for the considered systems, some information about PES can be obtained from the vibrational analysis. Here, we calculate vibrational frequencies at Γ -point using density functional perturbation theory. Most of the low-energy polymorphs are stable with respect to infinitesimal deformations at the fixed unit cell (Table S14). Among those with imaginary or prominently low frequencies is the relaxed experimental unit cell in both three- and two-dimensional forms. Recently, vibrational density of states (DOS) was used to distinguish polymorphs of P3HT.⁵ In agreement with that work, we observe substantial difference in DOS of structures distinct by a single dihedral, such as $CAab$ vs $CAabab$ or $CAaac$ vs $CAab$ (Figure S28). On the other hand, structures with the same side-chain conformation, such as $CAab$ vs $BAab$ or $CAaac$

vs $CBaac$, have very similar DOS except for that in the low-frequency region. The difference between three- and two-dimensional forms is even smaller (crystal vs π -stack in Figure S28). The calculated elasticity tensor (Table S15) is positive definite for low-energy structures, although the smallest eigenvalue is typically less than 1 GPa (it corresponds to XZ -deformation).

CONCLUSIONS

Establishing relationships between structure and electronic properties for organic semiconductors is pivotal for a number of optoelectronic technologies based on these materials. This task is complicated owing to materials' softness and multiple competing interactions ensuring a range of feasible and frequently coexisting chain packings spanning from highly ordered microcrystals to completely amorphous structures. Such diversity is of critical importance for optical and charge carrier transport properties. Even for the most studied P3HT polymer, available experimental and theoretical reports do not accurately resolve individual atom positions across packed microstructures in the bulk material. In the modeling arena, addressing this question requires a combination of a variety of electronic structure and classical MD approaches encompassing different scales. In addition, to account for enormous conformational variety of chain packings, structural modeling should be supplemented with an exhaustive and systematic search protocol for low-energy crystalline polymorphs. All of these components underscore our present modeling study.

Methodologically, we have performed extensive benchmarking of density functionals to CCSD(T) results for small P3HT fragments. In particular, we show that CAM-B3LYP-D3/6-311G* is among the most accurate computationally inexpensive DFT methods for P3HT, whereas PBE-MBD and vdW-DF2 functionals are accurate enough to be used for calculations with periodic boundary conditions. The generated symmetry-enumerated set of polymorphs can be further used as a seeding set for a more thorough search and for benchmarking of density functionals and force fields.

From our analysis, it follows that rr-P3HT is a statistically frustrated material in a sense that there are competing interatomic interactions of comparable strength but with inconsistent optimal geometries, which is typical for glass formers.⁷³ This leads to a broad variety of nearly isoenergetic geometries with distinct ordering. In particular, side-chain dihedrals alone prefer the trans-conformation but noncovalent interactions in P3HT environment minimize energy in folded conformations. The inter-ring dihedral prefers nonplanar conformation, but the π -stacking stabilizes the planar one. As a result of such frustration, we have about 10 lowest-energy high-symmetry two-dimensional π -stack polymorphs within the energy window of only 2 meV per atom, i.e., about 50 meV/monomer. All of these crystals have topologically different geometries and are kinetically stable at 200 K. In three dimensions, we naturally expect a combinatorially large number of nearly isoenergetic bulk structures, which can be obtained by piling up π -stacks on top of each other in the type-1 packing. Here, we do not observe any specific interstack interaction influencing intrastack structure so that the obtained ensemble of π -stacks should be representative of type-1 bulk P3HT.

All of the observed structures can be accurately parameterized by the proposed coarse-grained model involving 11 nearly independent degrees of freedom per monomer, including 3 translations, 3 rotations, and 5 dihedrals. The

lowest-energy polymorphs adopt a 2×2 unit cell with the smallest possible asymmetric unit. This symmetry can be broken at elevated energies and temperatures by slight modulation of monomer geometry. At room temperature, side chains melt into a glass former, although π -stacking order persists. Subsequently, we observe upon cooling a partially ordered structure corresponding to the so called "limit disordered" polymer model.⁹ This disorder should be taken into account in best-fit modeling of experimental structural data because existing "limit ordered" models do not correspond to a low-energy or thermally stable structure. A modeling of the room-temperature P3HT structure is currently limited by insufficient accuracy of available force fields. Using the published force field, at elevated temperatures, we have obtained four distinct semicrystalline π -stacks: two for parallel and two for antiparallel π -stacking. One of these two phases is a more ordered form of the other one, in agreement with the hypothesis suggested in ref 8.

We observe no preference between parallel and antiparallel stacking of P3HT chains. This should lead to a static disorder in self-assembled π -stacks, similar to that introduced by regiorandomness of P3HT chains. Consequently, it is interesting to see in practice if π -stack-regular P3HT would show an improved crystalline order. Another morphology with reduced disorder is a fully interdigitated one: it is substantially lower in energy than a type-1 structure, which however is stable at any temperature studied here.

In summary, this work provides a systematic modeling study of low-energy high-symmetry structures of bulk P3HT polymer. The obtained polymorphs can be used as a seeding set for a more comprehensive exploration of the configuration space, as a training set for optimization of density functionals and force fields, as well as for interpretation of experimental data with incompletely resolved molecular structure. Some of the two-dimensional structures can be energetically favorable in nonbulk forms,⁷⁴ in particular at oriented planar interfaces with well-ordered materials.^{75–77}

ASSOCIATED CONTENT

Supporting Information

The Supporting Information is available free of charge on the ACS Publications website at DOI: [10.1021/acs.jpcc.7b11271](https://doi.org/10.1021/acs.jpcc.7b11271).

Atomic coordinates for DFT-optimized polymorphs ([ZIP](#))

Details of structural analysis (Figure S1, Tables S1 and S2); structure prediction algorithm (Figures S2–S4); polyethylene oligomers (Tables S3 and S4, Figures S5–S7); elastic constants and vibrational frequencies (Tables S14 and S15, Figures S28 and S29) ([PDF](#))

AUTHOR INFORMATION

Corresponding Authors

*E-mail: a.zhugayevych@skoltech.ru. Phone: +7 495 2801481 (A.Z.).

*E-mail: serg@lanl.gov (S.T.).

ORCID

Andriy Zhugayevych: [0000-0003-4713-1289](https://orcid.org/0000-0003-4713-1289)

Sergei Tretiak: [0000-0001-5547-3647](https://orcid.org/0000-0001-5547-3647)

Notes

The authors declare no competing financial interest.

ACKNOWLEDGMENTS

This work is funded by Volkswagen Foundation (A115678). A.Z. acknowledges also financial support by Russian Science Foundation (16-13-00111). This work was performed, in part, at the Center for Integrated Nanotechnologies, an Office of Science User Facility operated for the U.S. Department of Energy (DOE) Office of Science by Los Alamos National Laboratory (Contract DE-AC52-06NA25396) and Sandia National Laboratories (Contract DE-AC04-94AL85000).

REFERENCES

- (1) Brinkmann, M.; Hartmann, L.; Kayunkid, N.; Djurado, D. In *P3HT Revisited - From Molecular Scale to Solar Cell Devices*; Ludwigs, S., Ed.; Springer: Berlin, 2014; pp 83–106.
- (2) Tremel, K.; Ludwigs, S. In *P3HT Revisited - From Molecular Scale to Solar Cell Devices*; Ludwigs, S., Ed.; Springer: Berlin, 2014; pp 39–82.
- (3) Wirix, M. J. M.; Bomans, P. H. H.; Friedrich, H.; Sommerdijk, N. A. J. M.; de With, G. Three-Dimensional Structure of P3HT Assemblies in Organic Solvents Revealed by Cryo-TEM. *Nano Lett.* **2014**, *14*, 2033–2038.
- (4) Agbolaghi, S.; Zenoozi, S. A Comprehensive Review on Poly(3-alkylthiophene)-based Crystalline Structures, Protocols and Electronic Applications. *Org. Electron.* **2017**, *51*, 362–403.
- (5) Harrelson, T. F.; Cheng, Y. Q.; Li, J.; Jacobs, I. E.; Ramirez-Cuesta, A. J.; Faller, R.; Moule, A. J. Identifying Atomic Scale Structure in Undoped/Doped Semicrystalline P3HT Using Inelastic Neutron Scattering. *Macromolecules* **2017**, *50*, 2424–2435.
- (6) Bohle, A.; Dudenko, D.; Koenen, N.; Sebastiani, D.; Allard, S.; Scherf, U.; Spiess, H. W.; Hansen, M. R. A Generalized Packing Model for Bulk Crystalline Regioregular Poly(3-alkylthiophenes) with Extended Side Chains. *Macromol. Chem. Phys.* **2017**, No. 1700266.
- (7) Kilina, S.; Batista, E. R.; Yang, P.; Tretiak, S.; Saxena, A.; Martin, R. L.; Smith, D. L. Electronic Structure of Self-Assembled Amorphous Polyfluorenes. *ACS Nano* **2008**, *2*, 1381–1388.
- (8) Panzer, F.; Sommer, M.; Bässler, H.; Thelakkat, M.; Köhler, A. Spectroscopic Signature of Two Distinct H-Aggregate Species in Poly(3-hexylthiophene). *Macromolecules* **2015**, *48*, 1543–1553.
- (9) De Rosa, C.; Auriemma, F. *Handbook of Polymer Crystallization*; Wiley, 2013; pp 31–72.
- (10) Xiao, X.; Wang, Z.; Hu, Z.; He, T. Single Crystals of Polythiophene with Different Molecular Conformations Obtained by Tetrahydrofuran Vapor Annealing and Controlling Solvent Evaporation. *J. Phys. Chem. B* **2010**, *114*, 7452–7460.
- (11) Kayunkid, N.; Uttiya, S.; Brinkmann, M. Structural Model of Regioregular Poly(3-hexylthiophene) Obtained by Electron Diffraction Analysis. *Macromolecules* **2010**, *43*, 4961–4967.
- (12) Dudenko, D.; Kiersnowski, A.; Shu, J.; Pisula, W.; Sebastiani, D.; Spiess, H. W.; Hansen, M. R. A Strategy for Revealing the Packing in Semicrystalline π-Conjugated Polymers: Crystal Structure of Bulk Poly-3-hexyl-thiophene (P3HT). *Angew. Chem., Int. Ed.* **2012**, *51*, 11068–11072.
- (13) Rivnay, J.; Mannsfeld, S. C. B.; Miller, C. E.; Salleo, A.; Toney, M. F. Quantitative Determination of Organic Semiconductor Microstructure from the Molecular to Device Scale. *Chem. Rev.* **2012**, *112*, S488–S519.
- (14) Lan, Y.-B.; Sher, P.-H.; Lee, C.-K.; Pao, C.-W.; Tsao, C.-S.; Huang, Y.-C.; Huang, P.-T.; Wu, C.-I.; Wang, J.-K. Revealing Ordered Polymer Packing during Freeze-Drying Fabrication of a Bulk Heterojunction Poly(3-hexylthiophene-2,5-diyl):[6,6]-Phenyl-C61-butyric Acid Methyl Ester Layer: In Situ Optical Spectroscopy, Molecular Dynamics Simulation, and X-ray Diffraction. *J. Phys. Chem. C* **2017**, *121*, 14826–14834.
- (15) Nieuwendaal, R. C.; Snyder, C. R.; DeLongchamp, D. M. Measuring Order in Regioregular Poly(3-hexylthiophene) with Solid-State ¹³C CP/MAS NMR. *ACS Macro Lett.* **2014**, *3*, 130–135.
- (16) Thurn-Albrecht, T.; Thomann, R.; Heinzel, T.; Hugger, S. Semicrystalline Morphology in Thin Films of Poly(3-Hexylthiophene). *Colloid Polym. Sci.* **2004**, *282*, 932–938.
- (17) Joshi, S.; Pingel, P.; Grigorian, S.; Panzner, T.; Pietsch, U.; Neher, D.; Forster, M.; Scherf, U. Bimodal Temperature Behavior of Structure and Mobility in High Molecular Weight P3HT Thin Films. *Macromolecules* **2009**, *42*, 4651–4660.
- (18) Wu, Z.; Petzold, A.; Henze, T.; Thurn-Albrecht, T.; Lohwasser, R. H.; Sommer, M.; Thelakkat, M. Temperature and Molecular Weight Dependent Hierarchical Equilibrium Structures in Semiconducting Poly(3-hexylthiophene). *Macromolecules* **2010**, *43*, 4646–4653.
- (19) Thankaraj Salammal, S.; Dai, S.; Pietsch, U.; Grigorian, S.; Koenen, N.; Scherf, U.; Kayunkid, N.; Brinkmann, M. Influence of Alkyl Side Chain Length on the In-Plane Stacking of Room Temperature and Low Temperature Cast Poly(3-Alkylthiophene) Thin Films. *Eur. Polym. J.* **2015**, *67*, 199–212.
- (20) Rahimi, K.; Botiz, I.; Stingelin, N.; Kayunkid, N.; Sommer, M.; Koch, F. P. V.; Nguyen, H.; Coulembier, O.; Dubois, P.; Brinkmann, M.; et al. Controllable Processes for Generating Large Single Crystals of Poly(3-hexylthiophene). *Angew. Chem., Int. Ed.* **2012**, *51*, 11131–11135.
- (21) Koch, F. P. V.; Heeney, M.; Smith, P. Thermal and Structural Characteristics of Oligo(3-hexylthiophene)s (3HT)_n, n = 4–36. *J. Am. Chem. Soc.* **2013**, *135*, 13699–13709.
- (22) Poelking, C.; Daoulas, K.; Troisi, A.; Andrienko, D. In *P3HT Revisited - From Molecular Scale to Solar Cell Devices*; Ludwigs, S., Ed.; Springer: Berlin, 2014; pp 139–180.
- (23) Alexiadis, O.; Mavrntzas, V. G. All-Atom Molecular Dynamics Simulation of Temperature Effects on the Structural, Thermodynamic, and Packing Properties of the Pure Amorphous and Pure Crystalline Phases of Regioregular P3HT. *Macromolecules* **2013**, *46*, 2450–2467.
- (24) Tummala, N. R.; Risko, C.; Bruner, C.; Dauskardt, R. H.; Brédas, J.-L. Entanglements in P3HT and Their Influence on Thin-Film Mechanical Properties: Insights from Molecular Dynamics Simulations. *J. Polym. Sci., Part B: Polym. Phys.* **2015**, *53*, 934–942.
- (25) Miura, T.; Ito, T.; Shimomura, T. Molecular Dynamics Simulation on the Nanofiber Formation of Conducting Polymers in Solutions. *Mol. Cryst. Liq. Cryst.* **2016**, *629*, 248–253.
- (26) Jones, M. L.; Jankowski, E. Computationally Connecting Organic Photovoltaic Performance to Atomistic Arrangements and Bulk Morphology. *Mol. Simul.* **2017**, *756*–773.
- (27) Xie, W.; Sun, Y. Y.; Zhang, S. B.; Northrup, J. E. Structure and Sources of Disorder in Poly(3-Hexylthiophene) Crystals Investigated by Density Functional Calculations with van der Waals Interactions. *Phys. Rev. B* **2011**, *83*, No. 184117.
- (28) Tsumuraya, T.; Song, J.-H.; Freeman, A. J. Linear Optical Properties and Electronic Structures of Poly(3-Hexylthiophene) and Poly(3-Hexylselenophene) Crystals From First Principles. *Phys. Rev. B* **2012**, *86*, No. 075114.
- (29) Marcon, V.; Raos, G. Molecular Modeling of Crystalline Oligothiophenes: Testing and Development of Improved Force Fields. *J. Phys. Chem. B* **2004**, *108*, 18053–18064.
- (30) Moreno, M.; Casalegno, M.; Raos, G.; Meille, S. V.; Po, R. Molecular Modeling of Crystalline Alkylthiophene Oligomers and Polymers. *J. Phys. Chem. B* **2010**, *114*, 1591–1602.
- (31) Poelking, C.; Andrienko, D. Effect of Polymorphism, Regioregularity and Paracrystallinity on Charge Transport in Poly(3-hexylthiophene) [P3HT] Nanofibers. *Macromolecules* **2013**, *46*, 8941–8956.
- (32) Bhatta, R. S.; Yimer, Y. Y.; Perry, D. S.; Tsige, M. Improved Force Field for Molecular Modeling of Poly(3-hexylthiophene). *J. Phys. Chem. B* **2013**, *117*, 10035–10045.
- (33) Łužny, W.; Piwowarczyk, K. Molecular Dynamics Simulations of Poly(Alkylthiophenes): An Overall View of Some Recent Results. *Synth. Met.* **2013**, *179*, 1–9.
- (34) Adler, T. B.; Werner, H.-J. An Explicitly Correlated Local Coupled Cluster Method For Calculations of Large Molecules Close to the Basis Set Limit. *J. Chem. Phys.* **2011**, *135*, No. 144117.

- (35) Werner, H.-J.; Knowles, P. J.; Knizia, G.; Manby, F. R.; Schütz, M. Molpro: a General-Purpose Quantum Chemistry Program Package. *Wiley Interdiscip. Rev.: Comput. Mol. Sci.* **2012**, *2*, 242–253.
- (36) Werner, H.-J.; Knowles, P. J.; Knizia, G.; Manby, F. R.; Schütz, M.; Celani, P.; Györffy, W.; Kats, D.; Korona, T.; et al. MOLPRO, version 2015.1, 2015. <http://www.molpro.net>.
- (37) Dunning, T. H. Gaussian Basis Sets for Use in Correlated Molecular Calculations. I. The Atoms Boron through Neon and Hydrogen. *J. Chem. Phys.* **1989**, *90*, 1007–1023.
- (38) Woon, D. E.; Dunning, T. H. J. Gaussian Basis Sets for Use in Correlated Molecular Calculations. III. The Atoms Aluminum through Argon. *J. Chem. Phys.* **1993**, *98*, 1358–1371.
- (39) Zhugayevich, A.; Postupna, O.; Wang, H.-L.; Tretiak, S. Modification of Optoelectronic Properties of Conjugated Oligomers due to Donor/Acceptor Functionalization: DFT Study. *Chem. Phys.* **2016**, *481*, 133–143.
- (40) Zhugayevich, A.; Tretiak, S. Theoretical Description of Structural and Electronic Properties of Organic Photovoltaic Materials. *Annu. Rev. Phys. Chem.* **2015**, *66*, 305–330.
- (41) Zhang, C.-R.; Sears, J. S.; Yang, B.; Aziz, S. G.; Coropceanu, V.; Bredas, J.-L. Theoretical Study of the Local and Charge-Transfer Excitations in Model Complexes of Pentacene-C₆₀ Using Tuned Range-Separated Hybrid Functionals. *J. Chem. Theory Comput.* **2014**, *10*, 2379–2388.
- (42) Grimme, S.; Hansen, A.; Brandenburg, J. G.; Bannwarth, C. Dispersion-Corrected Mean-Field Electronic Structure Methods. *Chem. Rev.* **2016**, *116*, 5105–5154.
- (43) Grimme, S.; Ehrlich, S.; Goerigk, L. Effect of the Damping Function in Dispersion Corrected Density Functional Theory. *J. Comput. Chem.* **2011**, *32*, 1456–1465.
- (44) Chai, J.-D.; Head-Gordon, M. Long-Range Corrected Hybrid Density Functionals with Damped Atom-Atom Dispersion Corrections. *Phys. Chem. Chem. Phys.* **2008**, *10*, 6615–6620.
- (45) Sure, R.; Brandenburg, J. G.; Grimme, S. Small Atomic Orbital Basis Set First-Principles Quantum Chem. Methods for Large Molecular and Periodic Systems: A Critical Analysis of Error Sources. *ChemistryOpen* **2016**, *5*, 94–109.
- (46) Frisch, M. J.; Trucks, G. W.; Schlegel, H. B.; Scuseria, G. E.; Robb, M. A.; Cheeseman, J. R.; Scalmani, G.; Barone, V.; Mennucci, B.; et al. Gaussian 09, revision A.1; Gaussian Inc.: Wallingford, CT, 2009.
- (47) Lee, K.; Murray, E. D.; Kong, L.; Lundqvist, B. I.; Langreth, D. C. Higher-Accuracy van der Waals Density Functional. *Phys. Rev. B* **2010**, *82*, No. 081101.
- (48) Klimeš, J.; Bowler, D. R.; Michaelides, A. Van der Waals Density Functionals Applied to Solids. *Phys. Rev. B* **2011**, *83*, No. 195131.
- (49) Ambrosetti, A.; Reilly, A. M.; DiStasio, R. A. J.; Tkatchenko, A. Long-Range Correlation Energy Calculated from Coupled Atomic Response Functions. *J. Chem. Phys.* **2013**, *140*, No. 18A508.
- (50) Perdew, J. P.; Yue, W. Accurate and Simple Density Functional For the Electronic Exchange Energy: Generalized Gradient Approximation. *Phys. Rev. B* **1986**, *33*, 8800–8802.
- (51) Murray, E. D.; Lee, K.; Langreth, D. C. Investigation of Exchange Energy Density Functional Accuracy for Interacting Molecules. *J. Chem. Theory Comput.* **2009**, *5*, 2754–2762.
- (52) Brown-Altvater, F.; Rangel, T.; Neaton, J. B. Ab Initio Phonon Dispersion in Crystalline Naphthalene Using van der Waals Density Functionals. *Phys. Rev. B* **2016**, *93*, No. 195206.
- (53) Pham, T. H.; Ramprasad, R.; Nguyen, H.-V. Density-Functional Description of Polymer Crystals: A Comparative Study of Recent van der Waals Functionals. *J. Chem. Phys.* **2016**, *144*, No. 214905.
- (54) Beran, G. J. O. Modeling Polymorphic Molecular Crystals with Electronic Structure Theory. *Chem. Rev.* **2016**, *116*, 5567–5613.
- (55) Perdew, J. P.; Burke, K.; Ernzerhof, M. Generalized Gradient Approximation Made Simple. *Phys. Rev. Lett.* **1996**, *77*, 3865–3868.
- (56) Kresse, G.; Furthmüller, J. Efficient Iterative Schemes for Ab Initio Total-Energy Calculations Using a Plane-Wave Basis Set. *Phys. Rev. B* **1996**, *54*, 11169–11186.
- (57) Kresse, G.; Joubert, D. From Ultrasoft Pseudopotentials to the Projector Augmented-Wave Method. *Phys. Rev. B* **1999**, *59*, 1758–1775.
- (58) Byrd, J. N.; Bartlett, R. J.; Montgomery, J. A. At What Chain Length do Unbranched Alkanes Prefer Folded Conformations? *J. Phys. Chem. A* **2014**, *118*, 1706–1712.
- (59) Busing, W. R. X-ray Diffraction Study of Disorder in Allied Spectra-1000 Polyethylene Fibers. *Macromolecules* **1990**, *23*, 4608–4610.
- (60) Siegrist, T.; Kloc, C.; Laudise, R. A.; Katz, H. E.; Haddon, R. C. Crystal Growth, Structure, and Electronic Band Structure of α -T Polymorphs. *Adv. Mater.* **1998**, *10*, 379–382.
- (61) Plimpton, S. Fast Parallel Algorithms for Short-Range Molecular Dynamics. *J. Comput. Phys.* **1995**, *117*, 1–19.
- (62) Jorgensen, W. L.; Maxwell, D. S.; Tirado-Rives, J. Development and Testing of the OPLS All-Atom Force Field on Conformational Energetics and Properties of Organic Liquids. *J. Am. Chem. Soc.* **1996**, *118*, 11225–11236.
- (63) Ponder, J. W. TINKER 7.1. <http://dasher.wustl.edu/tinker>.
- (64) Bitzek, E.; Koskinen, P.; Gähler, F.; Moseler, M.; Gumbsch, P. Structural Relaxation Made Simple. *Phys. Rev. Lett.* **2006**, *97*, No. 170201.
- (65) Brandenburg, J. G.; Grimme, S. Organic Crystal Polymorphism: a Benchmark for Dispersion-Corrected Mean-Field Electronic Structure Methods. *Acta Crystallogr., Sect. B: Struct. Sci., Cryst. Eng. Mater.* **2016**, *72*, 502–513.
- (66) Sharma, V.; Wang, C.; Lorenzini, R. G.; Ma, R.; Zhu, Q.; Sinkovits, D. W.; Pilania, G.; Oganov, A. R.; Kumar, S.; Sotzing, G. A.; et al. Rational Design of All Organic Polymer Dielectrics. *Nat. Commun.* **2014**, *5*, No. 4845.
- (67) Jones, M. L.; Huang, D. M.; Chakrabarti, B.; Groves, C. Relating Molecular Morphology to Charge Mobility in Semicrystalline Conjugated Polymers. *J. Phys. Chem. C* **2016**, *120*, 4240–4250.
- (68) Siu, S. W. I.; Pluhackova, K.; Böckmann, R. A. Optimization of the OPLS-AA Force Field for Long Hydrocarbons. *J. Chem. Theory Comput.* **2012**, *8*, 1459–1470.
- (69) Baggio, A.; Famulari, A. On the Inter-Ring Torsion Potential of Regioregular P3HT: a First Principles Reexamination with Explicit Side Chains. *Phys. Chem. Chem. Phys.* **2014**, *16*, 3983–3994.
- (70) Samdal, S.; Samuelsen, E. J.; Volden, H. V. Molecular Conformation of 2,2'-Bithiophene Determined by Gas Phase Electron Diffraction and Ab Initio Calculations. *Synth. Met.* **1993**, *59*, 259–265.
- (71) van der Poll, T. S.; Zhugayevich, A.; Chertkov, E.; Bakus, R. C.; Coughlin, J. E.; Teat, S. J.; Bazan, G. C.; Tretiak, S. Polymorphism of Crystalline Molecular Donors for Solution-Processed Organic Photovoltaics. *J. Phys. Chem. Lett.* **2014**, *5*, 2700–2704.
- (72) Coughlin, J. E.; Zhugayevich, A.; Bakus, R. C.; van der Poll, T. S.; Welch, G. C.; Teat, S. J.; Bazan, G. C.; Tretiak, S. A Combined Experimental and Theoretical Study of Conformational Preferences of Molecular Semiconductors. *J. Phys. Chem. C* **2014**, *118*, 15610–15623.
- (73) Zhugayevich, A.; Lubchenko, V. Electronic Structure and the Glass Transition in Pnictide and Chalcogenide Semiconductor Alloys. I. The Formation of the pp Sigma-Network. *J. Chem. Phys.* **2010**, *133*, No. 234503.
- (74) Diao, Y.; Lenn, K. M.; Lee, W.-Y.; Blood-Forsythe, M. A.; Xu, J.; Mao, Y.; Kim, Y.; Reinsch, J. A.; Park, S.; Aspuru-Guzik, A.; et al. Understanding Polymorphism in Organic Semiconductor Thin Films through Nanoconfinement. *J. Am. Chem. Soc.* **2014**, *136*, 17046–17057.
- (75) Jones, A. O. F.; Chattopadhyay, B.; Geerts, Y. H.; Resel, R. Substrate-Induced and Thin-Film Phases: Polymorphism of Organic Materials on Surfaces. *Adv. Funct. Mater.* **2016**, *26*, 2233–2255.
- (76) Zhai, L.; Khondaker, S. I.; Thomas, J.; Shen, C.; McInnis, M. Ordered Conjugated Polymer Nano- and Microstructures: Structure Control for Improved Performance of Organic Electronics. *Nano Today* **2014**, *9*, 705–721.
- (77) Anokhin, D. V.; Leshanskaya, L. I.; Piryazev, A. A.; Susarova, D. K.; Dremova, N. N.; Shcheglov, E. V.; Ivanov, D. A.; Razumov, V. F.; Troshin, P. A. Towards Understanding the Behavior of Indigo Thin

Films in Organic Field-Effect Transistors: a Template Effect of the Aliphatic Hydrocarbon Dielectric on the Crystal Structure and Electrical Performance of the Semiconductor. *Chem. Commun.* **2014**, *50*, 7639–7641.

Supporting Information for

“Lowest-Energy Crystalline Polymorphs of P3HT”

Andriy Zhugayevych,[†] Olga Mazaleva,[†] Artem Naumov,[†] Sergei Tretiak^{‡,†}

[†] *Skolkovo Institute of Science and Technology, Moscow 143026, Russia*

[‡] *Theoretical Division and Center for Integrated Nanotechnologies, Los Alamos National Laboratory, NM 87545, United States*

E-mail: a.zhugayevych@skoltech.ru; serg@lanl.gov

March 27, 2018

S1	Details of structural analysis	S2
S2	Structure prediction algorithm	S5
S3	Polyethylene oligomers	S7
S4	Polythiophene oligomers	S10
S5	P3HT monomer	S11
S6	Crystals with resolved structure: polyethylene, oligothiophenes, P3HT	S15
S7	Low-energy polymorphs by force field	S16
S8	Low-energy polymorphs by DFT	S19
S9	Elastic constants and vibrational frequencies	S26
S10	Electronic structure	S29
S11	Selected tables recalculated in kcal/mol energy unit	S30

S1 Details of structural analysis

To separate large scale deformations from the local ones, we use the local basis defined by the regular two-dimensional grid approximating (in the least squares sense) centers of thiophene rings for a set of monomers. More specifically, we take a 5×5 grid centered at a given monomer with weight 1/2 for sides and 1/4 for corners (to smooth out finite size effects). Then the monomer position and orientation are calculated in this local coordinate system. Since we are not interested in such high energy processes as side-chain flips in x and y axes, we use two topological signs to denote the x and y orientations as shown in Fig. S1, while measuring Euler's angles relative to this orientation. Also to keep the angles small we define them in such a way that the transformation matrix from the canonical orientation is given by $SR_x(-\phi)R_y(\theta)R_z(-\psi)$, where R are rotation matrices around the corresponding axes and S is the diagonal matrix with the elements ± 1 . Without the loss of generality we put $S_{zz} \equiv S_z = S_xS_y$ so that we have a proper rotation. The two remaining parameters $S_{x,y} = \pm 1$ are topological constants. We also introduce the so-called setting angle $\varphi \equiv S_x\phi$, whose sign is defined in the global coordinate system.

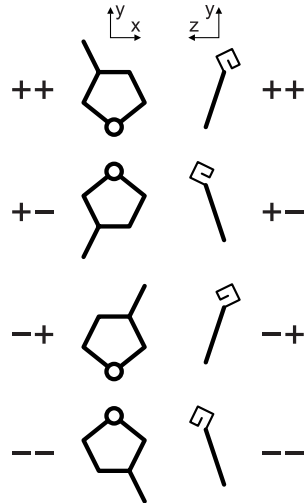


Figure S1: Monomer orientation notations. Two signs on the left encode orientation of the side-chain in xy -plane: forward-backward (sign 1) and up-down (sign 2). Two signs on the right correspond to sign of the determinant transforming the monomer to a reference structure (sign 3) and sign of the setting angle (sign 4). Note that signs 1-3 are topological for any molecular dynamics considered in this work.

Table S1: Example of a coarse-grained representation of a semicrystalline P3HT. Here a 4×4 block of amorphous structure a-*C_Ba* shown in Fig. S16 is given in the coarse-grained coordinates ($x, y, z, \phi, \theta, \psi, \delta_1 \dots \delta_5$). The indices (i, j) enumerate monomers within the block. The next column shows monomer codes consisting of four signs \pm describing orientation of the thiophene ring as defined in Fig. S1 followed by five letters describing conformation of the side chain as defined in the main text. The last column is RMSD between the actual monomer geometry and the geometry obtained from a reference monomer (planar polymer optimized by CAM-B3LYP/6-31G*) by setting all 11 coarse-grained coordinates to their actual values. The RMSD and coordinates x, y, z are given in Å, other coordinates are angles given in degrees.

(i, j)	code	x	y	z	ϕ	θ	ψ	δ_1	δ_2	δ_3	δ_4	δ_5	RMSD
(1,1)	++++aaaaaa	0.13	0.39	-0.04	20.8	-0.0	0.4	95	-155	177	-176	-178	0.69
(2,1)	----baaaa	0.14	-0.44	-0.02	21.6	0.7	2.9	100	178	180	177	179	0.71
(3,1)	++++aaaaaa	0.12	0.54	0.02	20.8	1.1	1.4	88	-155	174	-175	-175	0.45
(4,1)	----bbaaaa	0.11	-0.42	-0.02	20.7	1.1	0.9	105	83	-174	-177	-174	0.67
(1,2)	---+bbaaaa	-0.25	0.45	-0.07	21.7	1.3	2.8	110	85	-173	-179	-177	0.65
(2,2)	---+aabaaa	-0.24	-0.40	0.01	23.3	2.2	0.8	104	-169	-55	-177	-175	0.76
(3,2)	---+baccaa	-0.26	0.56	0.06	21.5	-0.2	2.4	101	-177	-63	-174	-178	0.67
(4,2)	---+aaaaaa	-0.24	-0.31	0.01	20.1	-0.0	0.4	93	-154	178	-176	-178	0.68
(1,3)	++++aaaaaa	0.20	0.33	-0.08	21.6	0.1	0.6	92	-157	-179	-175	-179	0.32
(2,3)	----bbaaab	0.23	-0.51	-0.03	22.2	0.4	2.9	107	84	172	-178	73	0.69
(3,3)	++++aaccaa	0.21	0.49	0.04	19.5	0.6	1.0	96	-177	82	177	-172	0.66
(4,3)	----baccaa	0.22	-0.43	0.03	21.1	-0.4	1.8	99	-171	-63	-170	-175	0.69
(1,4)	---+bbbaaa	-0.12	0.48	-0.07	23.1	1.5	3.1	110	81	180	-175	-175	0.66
(2,4)	---+aaccaa	-0.12	-0.42	-0.02	18.4	1.3	2.1	98	-180	76	-179	-175	0.65
(3,4)	---+baaab	-0.10	0.45	0.01	20.9	0.8	0.6	91	-161	173	-179	69	0.73
(4,4)	---+aaccaa	-0.12	-0.55	0.00	21.2	0.2	2.6	99	-175	78	174	-173	0.25

Table S2: Possible structural types of 2×2 unit cell with the smallest asymmetric unit (single monomer). Lattice centering “b” is generated by $(x, y + 1/2, z)$. Transformation matrices are given by Eq. (S1). Lattice types are abbreviated as (m)onoclinic or (o)rthorhombic vs. (o)blique or (r)eangular.

code	signs	group	trans.	lattice
AA	+++ +	b2 ₁ 11	xz	m/r
AB	+++-	b11a	xz	m/o
AC	++-+	pm2 ₁ n	zx	o/r
AD	++--	pm2 ₁ b	zx	o/r
BA	+ - ++	c211	xz	m/r
BB	+ - +-	pb2b	zx	o/r
BC	+ -- +	pb2 ₁ a	zxZ	o/r
BD	+ ---	c11a	xz	m/o
CA	- + ++	p2 ₁ /b11	xz	m/r
CB	- + +-	pb2 ₁ a	xz	o/r
CC	- + - +	p2 ₁ 2 ₁ 2	zxX	o/r
CD	- + --	p112/a	xz	m/o
DA	-- + +	p2 ₁ /b11	xzX	m/r
DB	-- + -	p112/a	xzX	m/o
DC	-- - +	p2 ₁ 2 ₁ 2	zx	o/r
DD	-- - -	pb2 ₁ a	xzX	o/r
B	+ ± 0 0	pbma	xz	o/r
C	- ± 0 0	cm2e	zx	o/r

$$zx = \begin{pmatrix} 0 & 0 & 1 \\ 1 & 0 & 0 \\ 0 & 1 & 0 \end{pmatrix}, \quad xz = \begin{pmatrix} 1 & 0 & 0 \\ 0 & 0 & 1 \\ 0 & 1 & 0 \end{pmatrix}, \quad zxX = \begin{pmatrix} 0 & 0 & 1 & 0 \\ 1 & 0 & 0 & 1/4 \\ 0 & 1 & 0 & 0 \end{pmatrix},$$

$$zxZ = \begin{pmatrix} 0 & 0 & 1 & 1/4 \\ 1 & 0 & 0 & 0 \\ 0 & 1 & 0 & 0 \end{pmatrix}, \quad xzX = \begin{pmatrix} 1 & 0 & 0 & 1/4 \\ 0 & 0 & 1 & 0 \\ 0 & 1 & 0 & 0 \end{pmatrix} \quad (\text{S1})$$

S2 Structure prediction algorithm

The search starts from combinatorial generation of a set of low-energy crystals followed by their geometry relaxation. These crystals are then equilibrated at some temperature followed by a rapid quench, i.e., the temperature is reduced to nearly zero within nanoseconds. The resulting structures are scanned for most common 2×2 motifs using the above described algorithm. Applied iteratively, this approach allows for a comprehensive study of low-energy polymorphs including amorphous ones. The seeding set consists of all combinations of 16 lattice types and 22 side-chain conformations, including all possible values of $\delta_{1,2,3}$ (18 conformers) plus geometrically uncrowded combinations with δ_4 (*abab*, *acac*, *bbab*, *bcac*). Conformational space of the terminal part of side chains (at least δ_5) is properly sampled during MD. We use two MD setups. In the first one, we run 10 ns MD at fixed temperature for a double cell (4×4 monomers). In the second setup, we take a large supercell (16×16 monomers) and apply melt-equilibrate-quench approach to investigate stability of structures and transformation between them. The temperature-change profile is trapezium-shaped, see Fig. S2. Each stage takes about 1 ns (< 1 K/ps when heating or cooling) to maintain quasi-equilibrium (at least locally) as evidenced by trapezium-shaped time dependence of energy and volume, see Fig. S3. To compare, previous study¹ used 4 ns timescale to anneal amorphous P3HT.

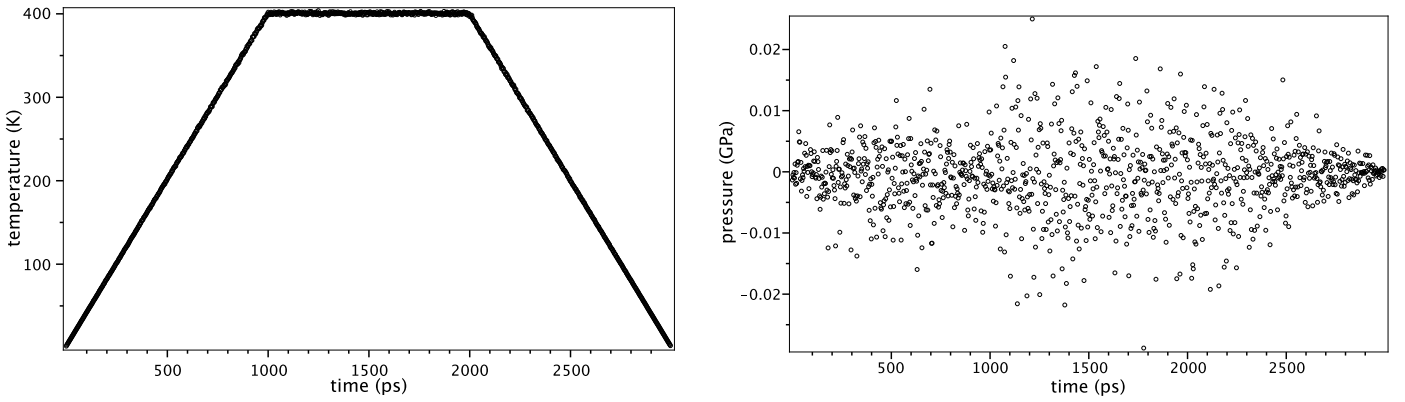


Figure S2: Temperature and pressure profiles for 1-400-400-1 K melt-equilibrate-quench MD for *CBaac* π -stack in 16×16 supercell.

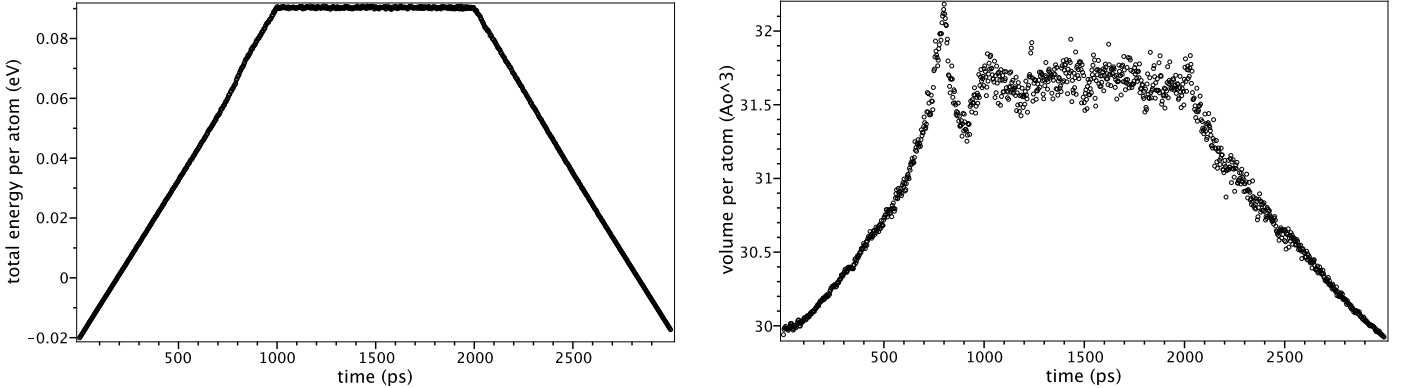


Figure S3: Total energy and volume profiles for the system described in Fig. S2.

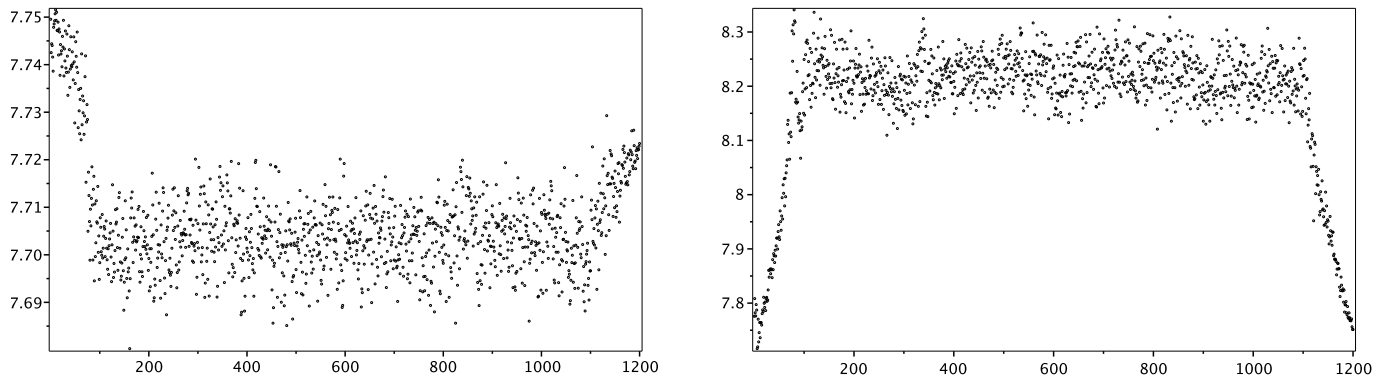


Figure S4: Mean translation periods along polymer (left panel) and π -stack (right panel) directions for the system described in Fig. S2. Note that the melt and quench stages are recorded 10 times more sparsely than the equilibration stage, resulting in their compressed visual representation. In other words, horizontal tickmark 100 corresponds to 1000 ps, 1100 to 2000 ps, and 1200 to 3000 ps.

S3 Polyethylene oligomers

Table S3: Basis size dependence of the relative energy (hairpin minus trans) of the largest considered polyethylene oligomer (18 carbons). The reference CCSD(T)/cc-pvTZ value is -73 meV.

Basis set	size	N_{prim}	CAM-B3LYP	B3LYP	LC- ω PBE	ω WB97X
6-31G*	346	656	-104	-141	-128	-206
6-311G*	438	766	-72	-98	-140	-215
6-31G**	460	770	-106	-143	-136	-220
6-311G**	552	880	-86	-114	-149	-229
6-31G(2d,p)	568	878	-103	-145	-123	-212
6-31+G(2d,p)	640	950	-45	-86	-88	-178
6-311G(2d,p)	642	988	-72	-105	-127	-210
6-311+G(2d,p)	714	1060	-65	-96	-119	-203
6-311+G(3df,2p)	1044	1462	-75	-106	-127	-207

Table S4: Comparison of different methods estimating the relative, hairpin minus trans, energy for a set of polyethylene oligomers (8 to 18 carbons). The geometry is fixed at MP2/cc-pvTZ geometry obtained in Ref.,² except for the last block in the table. The entries correspond to energies in meV. Here σ is RMSD with respect to the reference method which is CCSD(T)/cc-pVTZ.² “Optimized OPLS” means optimized C-C-C-C dihedral. The supercell size for plane waves is $40 \times 20 \times 20 \text{ \AA}$. See also graphical representation in Fig. S5.

σ	8	10	12	14	16	18	
Reference data							
CCSD-T/cc-pVTZ	0	65	52	37	5	-30	-73
6-311G*							
CAM-B3LYP-D3	5	71	61	42	10	-30	-72
B3LYP-D3	16	60	50	31	-12	-53	-98
vdW-DF2	19	90	83	62	14	-31	-71
PBE-MBD	22	66	55	34	-21	-62	-108
LC-wPBE-D3	50	29	15	-5	-47	-88	-140
wB97XD	90	24	11	-10	-95	-145	-215
CAM-B3LYP	195	138	143	148	227	222	227
6-311+G(3df,2p)							
CAM-B3LYP-D3	10	78	67	49	7	-33	-75
B3LYP-D3	21	65	54	36	-20	-61	-106
LC-wPBE-D3	39	41	29	10	-39	-77	-127
wB97XD	84	33	20	1	-90	-138	-207
CAM-B3LYP-D3							
6-311G*	5	71	61	42	10	-30	-72
6-311G**	8	68	57	38	-2	-43	-86
6-311+G(3df,2p)	10	78	67	49	7	-33	-75
6-311G(2d,p)	10	78	68	49	9	-30	-72
6-311+G(2d,p)	14	82	72	54	16	-23	-65
6-31G(2d,p)	18	73	61	37	-11	-56	-103
6-31G*	19	66	56	33	-12	-58	-104
6-31G**	20	67	57	34	-14	-59	-106
6-31+G(2d,p)	29	94	84	67	34	-4	-45
Geometry relaxed with the same method							
CAM-B3LYP-D3	4	67	57	38	4	-36	-79
optimized OPLS	8	54	41	27	3	-34	-72
B3LYP-D3	18	56	45	25	-14	-55	-100
LC-wPBE-D3	51	28	15	-6	-49	-88	-141
wB97XD	96	21	8	-13	-103	-154	-223
OPLS	118	160	161	149	135	97	58
CAM-B3LYPp3p	128	127	129	128	128	128	128

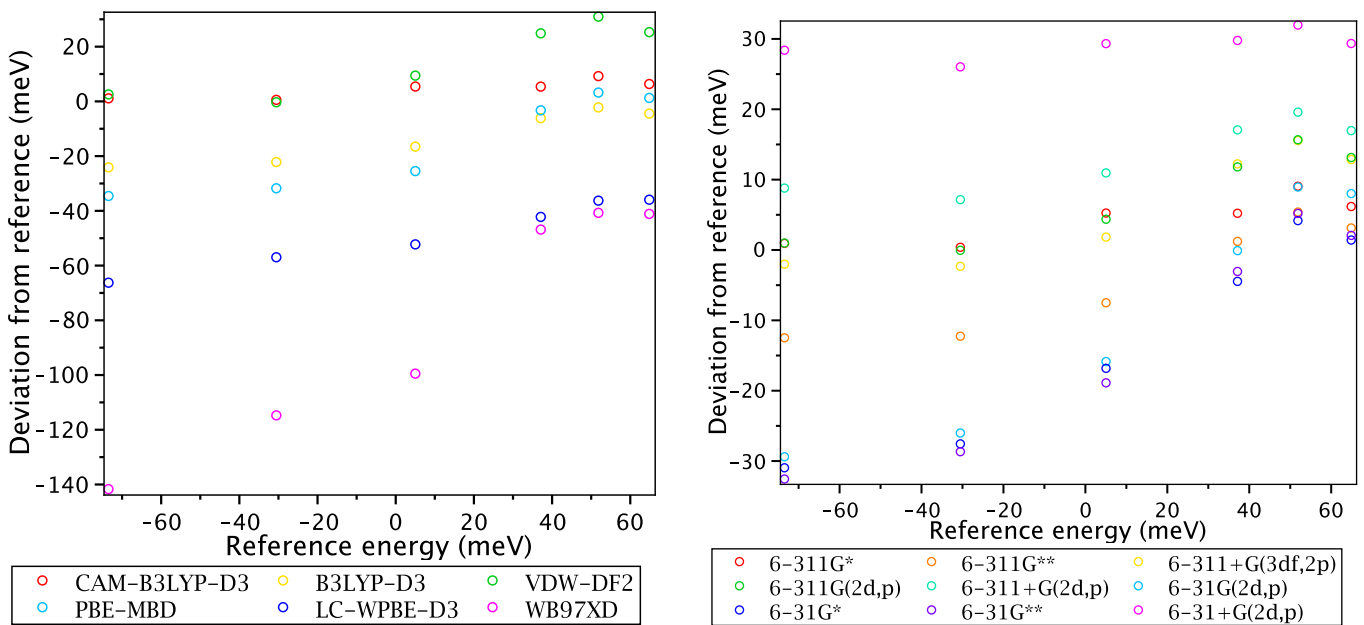


Figure S5: Graphical representation of Table S4: left panel – dependence on density functional, right panel – dependence on basis set.

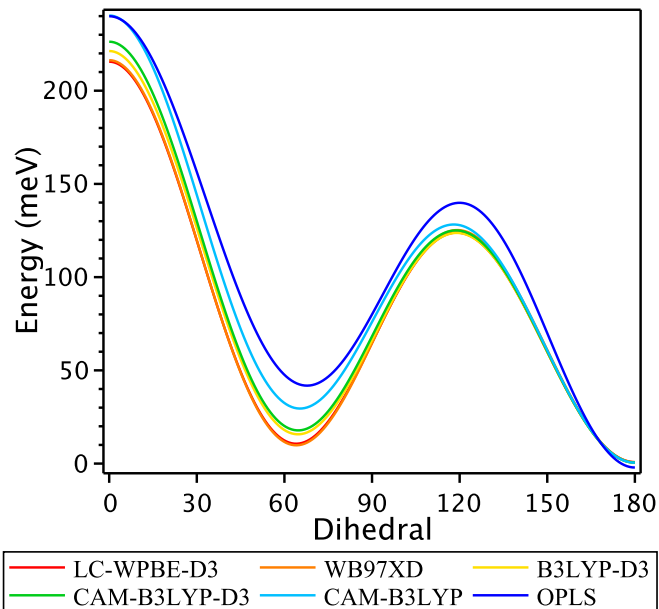


Figure S6: PES for the central dihedral in 8-carbon oligomer of polyethylene calculated by different methods.

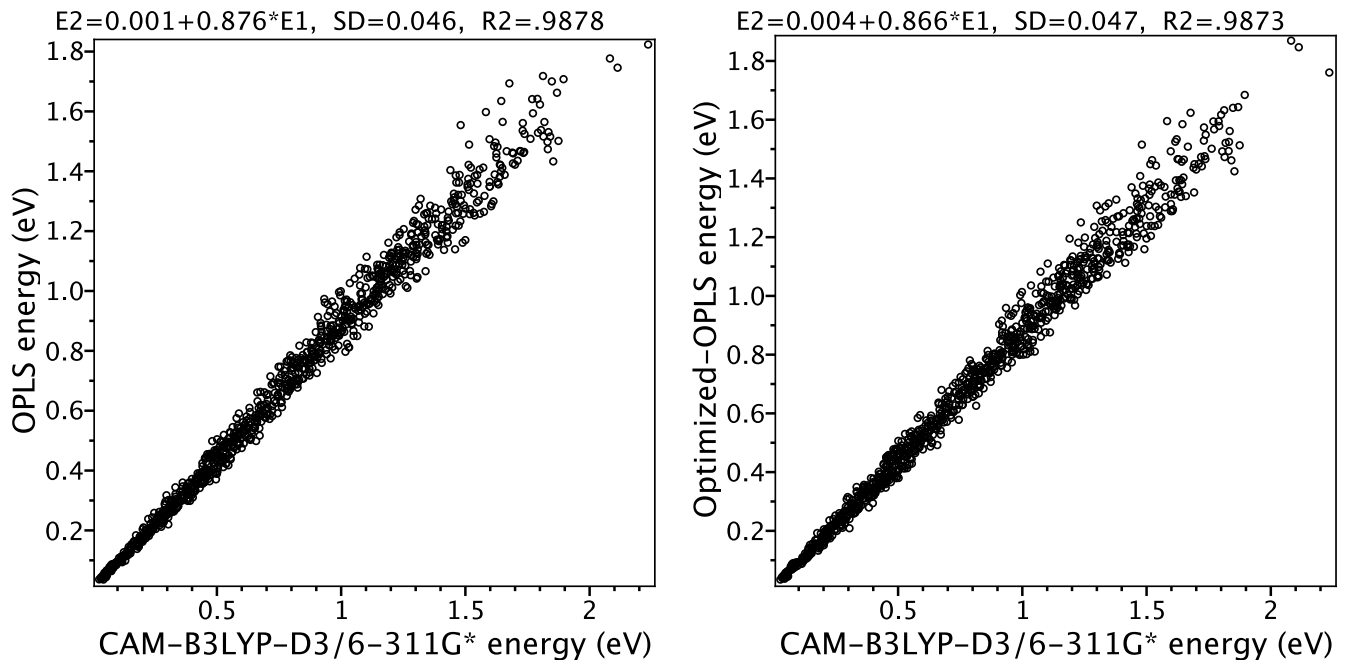


Figure S7: Accuracy of the OPLS force field for a set of molecular geometries sampling classical MD with a linear temperature increase from 10 to 400 K in 10 ns. Here ‘SD’ means standard deviation and ‘R²’ is the coefficient of determination.

Table S5: Intermolecular interaction energies (in meV per carbon atom) in polyethylene crystal.

structure	symmetry	PBE-MBD	vdW-DF2
stacking slab	pmam	28	28
side-to-side slab	cmma	48	46
high-symmetry crystal	Cmma	92	96
monoclinic crystal	C2/m	97	98
orthorhombic crystal	Pnma	99	100

S4 Polythiophene oligomers

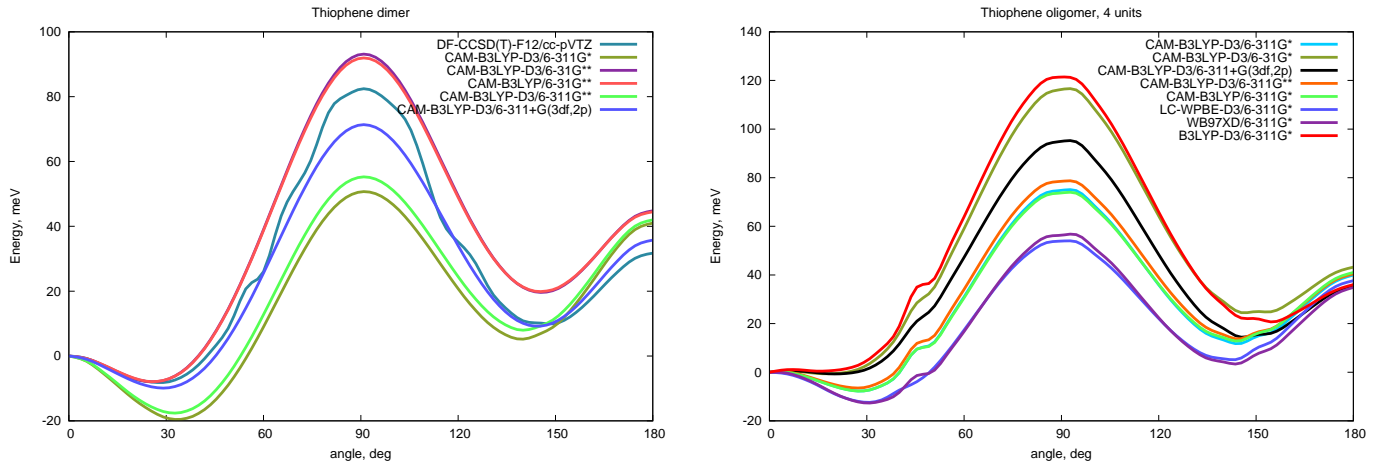


Figure S8: PES for central inter-ring dihedral in oligothiophenes calculated by different methods: dimer (left panel) and tetramer (right panel). Zero dihedral corresponds to trans conformation. According to experiment at 370 K the equilibrium values of dihedrals are $32(3)^\circ$ and $144(5)^\circ$ with 8 meV free energy difference between the two minima.³

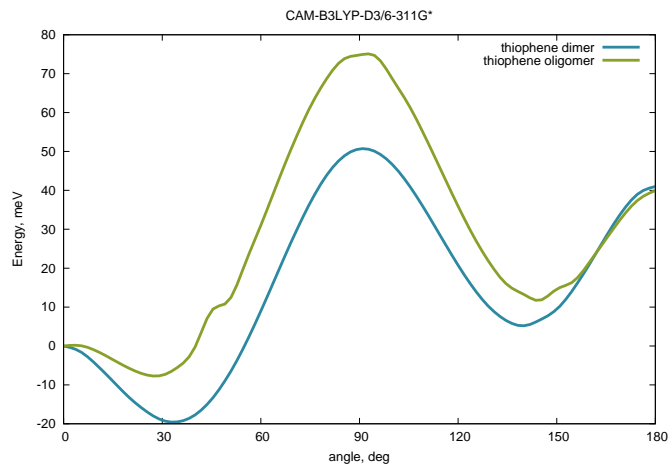


Figure S9: PES for central inter-ring dihedral in oligothiophenes: dependence on oligomer size.

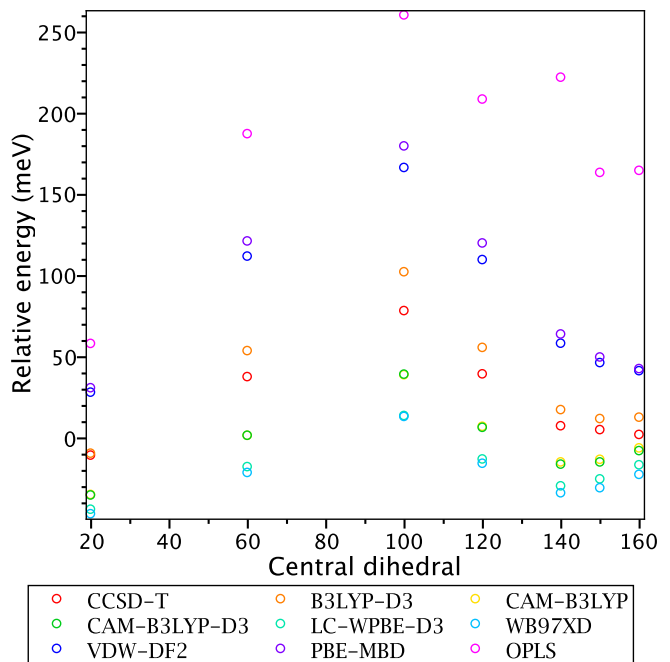


Figure S10: Energies of a set of tetramer conformers relative to the all-trans planar conformation. In Table 2 of the main text the standard deviation is divided by 3 because there are three sampled dihedrals.

S5 P3HT monomer

Table S6: Comparison of different methods estimating the energies of a set of 72 conformers of P3HT monomer relative to the energy of ‘a’-conformer. Notations for conformers are given in the main text except for ‘p’-conformer corresponding to $\delta = 180^\circ$, ‘ \bar{p} ’-conformer corresponding to $\delta = 0$, and ‘s’-conformer corresponding to the saddle point between ‘a’- and ‘p’-conformers. All entries are energies in meV. Here σ is RMSD with respect to the reference method which is CCSD(T)/cc-pVTZ. The default basis set is 6-311G* except for plane-wave based methods.

	σ	ab	abb	ac	acc	abab	abaab	\bar{p}	aac	s	p
Geometry fixed at CAM-B3LYP-D3/6-311G*											
CCSD-T/cc-pVTZ	0	-18	-17	-5	2	5	5	11	23	35	62
CAM-B3LYP-D3	5	-21	-17	3	11	4	3	13	22	40	69
B3LYP-D3	12	-25	-26	-3	-0	-3	-3	17	20	41	70
PBE-MBD	13	-10	-1	9	17	15	15	10	22	31	50
vdW-DF2	17	-7	2	12	21	17	17	30	24	39	74
LC-wPBE-D3	24	-34	-43	-8	-11	-15	-16	6	17	39	62
wB97XD	26	-27	-36	-6	-11	-10	-11	12	16	39	63
CAM-B3LYP	64	7	40	31	67	44	41	13	34	40	68
Dependence on basis set for CAM-B3LYP-D3 (fixed geometry)											
6-31G*	6	-20	-19	3	10	3	3	14	21	39	68
6-311G**	6	-22	-21	3	8	0	0	14	21	40	69
6-311+G(3df,2p)	12	-14	-6	10	20	12	11	14	24	38	67
Fully relaxed geometry at 6-31G**											
B3LYP-D3	12	-25	-26	-3	-0	-3	-3	17	20	41	70
PBE-MBD	13	-10	-1	9	17	15	15	10	22	31	50
vdW-DF2	15	-8	0	11	20	15	16	29	24	39	74
LC-wPBE-D3	27	-35	-45	-9	-13	-17	-17	6	17	39	62
wB97XD	27	-27	-37	-6	-11	-10	-11	12	16	39	63
OPLS	56	-1	37	15	50	40	38	20	46	44	72

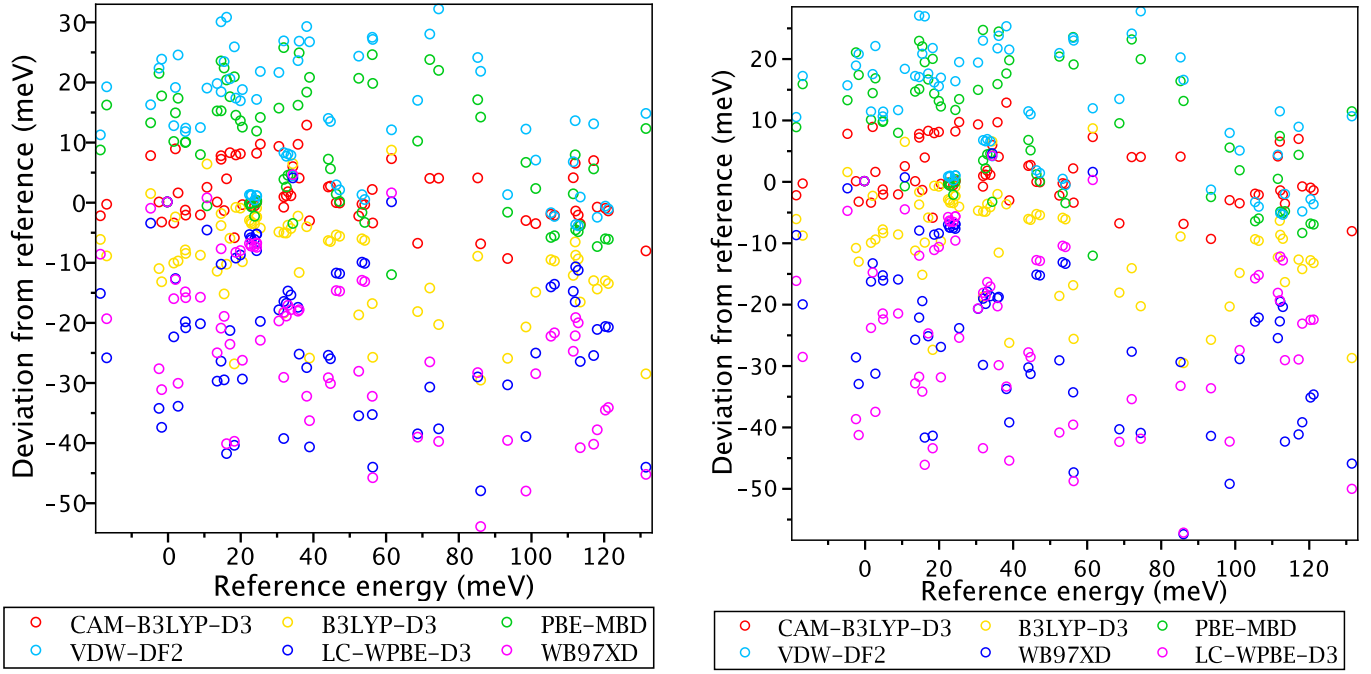


Figure S11: Accuracy of different methods: left panel – geometry fixed at CAM-B3LYP-D3/6-311G*, right panel – relaxed geometry. The reference method is CCSD(T)/cc-pVTZ, the basis set is 6-311G*.

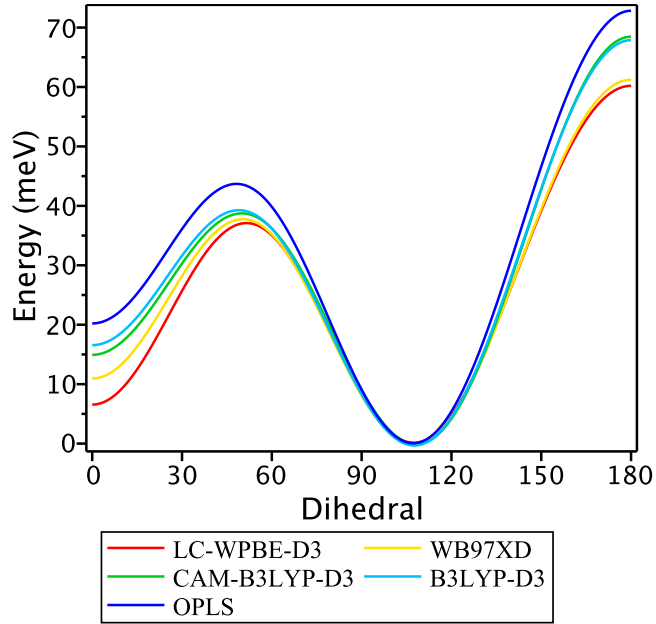


Figure S12: Accuracy of different methods for the dihedral δ_1 .

Table S7: Comparison of geometries for a set of 72 conformers of P3HT monomer optimized by different methods based on RMSD from reference geometries, which are optimized by CAM-B3LYP-D3/6-31G*. All values are in Å. The column “RMS” means root mean square of 72 RMSD of each conformer. The default basis set is 6-31G* except for plane-wave based methods.

	RMS	median	min	max
PBE-MBD	.011	.011	.011	.015
vdW-DF2	.027	.026	.023	.035
B3LYP-D3	.030	.020	.012	.135
wB97XD	.053	.040	.004	.179
LC-wPBE-D3	.091	.060	.014	.256
OPLS	.167	.126	.027	.436

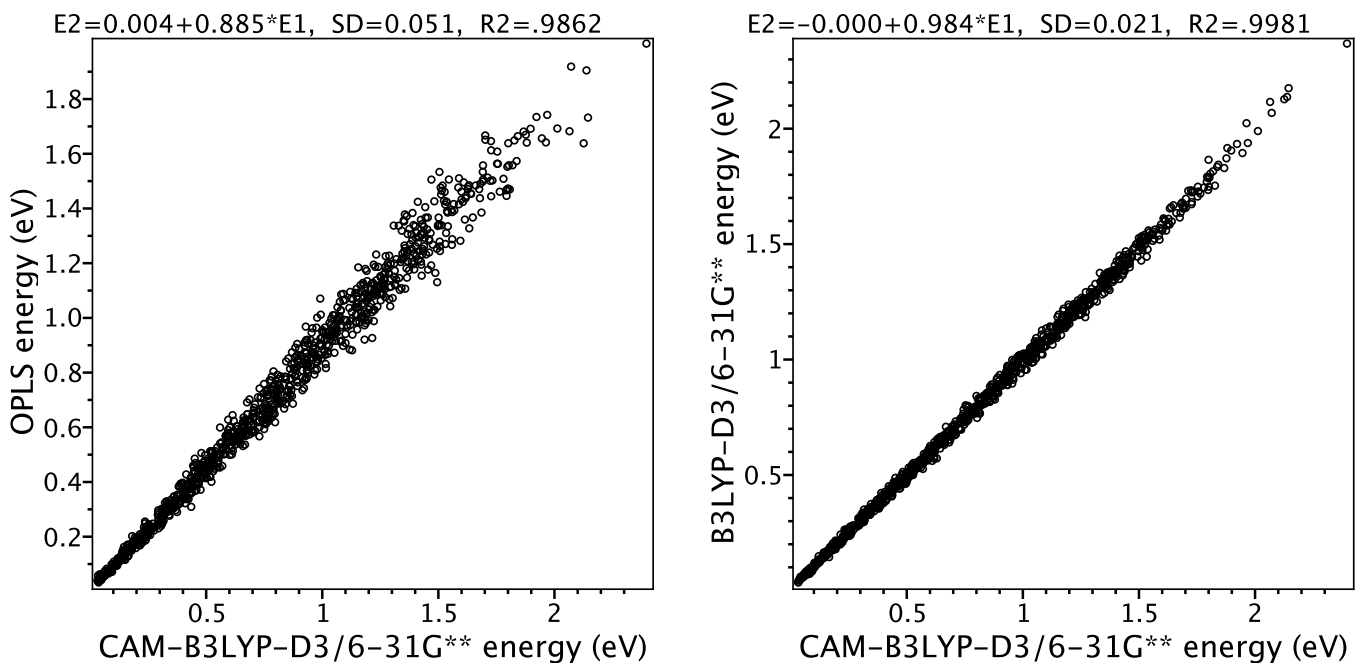


Figure S13: Accuracy of the force field compared to B3LYP-D3. Here ‘SD’ means standard deviation and ‘R2’ is the coefficient of determination. Molecular geometries are sampled from classical MD with a linear temperature increase from 10 to 400 K in 10 ns.

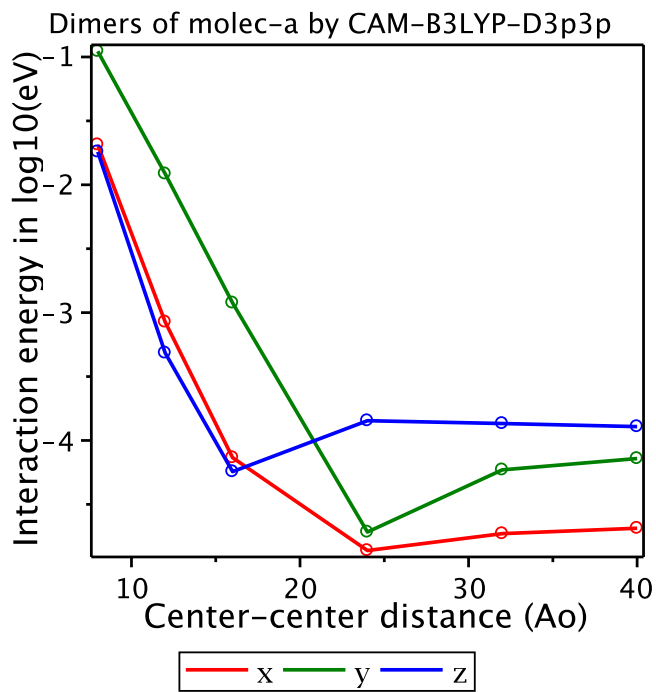


Figure S14: Distance dependence of intermolecular interaction energy for a pair of P3HT monomers separated along x , y , and z directions. At the chosen supercell size, 20 Å, the interaction is negligible.

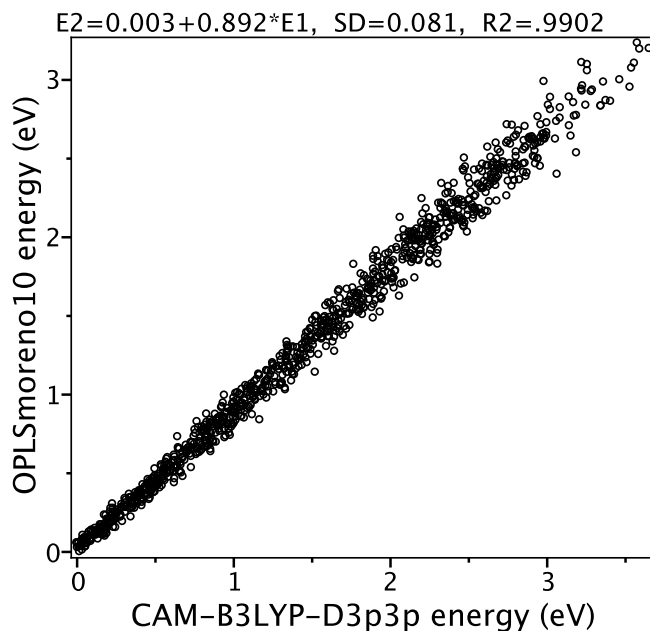


Figure S15: Accuracy of the force field for the P3HT dimer with molecular geometries sampled from classical MD with a linear temperature increase from 10 to 400 K in 10 ns.

S6 Crystals with resolved structure: polyethylene, oligothiophenes, P3HT

Table S8: Comparison of calculated and observed crystal structures relevant for P3HT. All experimental data are measured at room temperature. Here V is the volume per atom, $a, b, c, \alpha, \beta, \gamma$ are unit cell parameters in Å and degrees, $\Delta\xi$ is relative shift between two polymers/oligomers in π -stack, φ is angle between the π -stacking direction and the normal to the polymer plane (setting angle). The low-symmetry polymorph of rr-P3HT is lower in energy only by 0.23 meV/monomer, the low-temperature form of quarterthiophene is lower in energy by 21 meV/molecule for PBE-MBD and 14 meV/molecule for vdW-DF2 functionals.

method	V	a	b	c	α	β	γ	$\Delta\xi$	φ
Polyethylene, orthorhombic Pmcn									
Ref. ⁴	7.79	2.551	4.949	7.407	90	90	90	0	45.9
PBE-MBD	6.97	2.552	4.686	6.991	90	90	90	0	45.9
vdW-DF2	7.58	2.579	4.994	7.065	90	90	90	0	44.2
Quarterthiophene, low-temperature form P2 ₁ /c									
Ref. ⁵	12.14	6.085	7.858	30.483	90	91.81	90	0.58	61.3
PBE-MBD	11.94	5.959	7.886	30.500	90	91.34	90	0.56	60.9
vdW-DF2	12.39	6.026	8.000	30.858	90	91.39	90	0.56	61.4
Quarterthiophene, high-temperature form P2 ₁ /a									
Ref. ⁵	12.18	8.935	5.751	14.340	90	97.22	90	0.16	62.4
PBE-MBD	12.00	8.903	5.718	14.257	90	97.30	90	0.17	62.3
vdW-DF2	12.43	8.998	5.764	14.505	90	97.59	90	0.18	63.0
Interdigitated rr-P3HT, P2 ₁ /c11									
Ref. ⁶	8.80	7.770	12.900	9.440	68.50	90	90	0.08	42.6
PBE-MBD	8.65	7.799	13.301	8.879	69.91	90	90	0.26	38.1
vdW-DF2	9.06	7.890	13.534	9.065	69.32	90	90	0.26	37.6
Interdigitated rr-P3HT, low-symmetry P $\bar{1}$									
vdW-DF2	9.03	7.888	13.517	9.059	69.32	90.74	89.59	0.29	38.0

Table S9: Detailed comparison of calculated and observed P3HT crystals in coarse-grained coordinates. Here the last column is RMSD between the actual monomer geometry and the coarse-grained geometry based on planar polymer optimized by CAM-B3LYP/6-31G*. The RMSD and coordinates x, y, z are given in Å, other coordinates are angles given in degrees. Optimized type-1 crystals are relaxed from structure of Ref.⁷

method	code	x	y	z	ϕ	θ	ψ	δ_1	δ_2	δ_3	δ_4	δ_5	RMSD
Type-1 crystal, P2 ₁ /c11													
Ref. ⁸	CA	-0.74	0.36	-0.21	31.9	2.2	0.5	131	-133	173	-179	180	1.14
Ref. ⁷	DA	0.63	0.47	0.00	0.3	0.0	2.1	150	-134	180	-180	180	0.39
OPLS	CA	-0.91	0.48	0.08	-9.6	0.9	2.6	167	-169	-178	-177	-175	0.10
vdW-DF2	CA	-0.84	0.45	0.10	-12.6	0.5	2.7	162	-161	-179	-170	-178	0.12
PBE-MBD	CA	-0.80	0.46	0.07	-9.2	0.3	2.4	165	-164	178	-168	179	0.16
Type-2 crystal, P2 ₁ /c11													
Ref. ⁶	DAa	-0.16	0.35	-0.31	42.6	2.5	2.7	97	175	-175	180	-180	0.35
OPLS	DAa	-0.64	0.38	-0.30	35.9	-2.1	2.8	98	150	-173	179	-174	0.42
vdW-DF2	DAa	-0.51	0.36	-0.29	37.6	-1.3	3.0	94	159	-175	174	-177	0.62
PBE-MBD	DAa	-0.50	0.36	-0.30	38.1	-1.8	3.0	95	158	-174	174	-176	0.60

S7 Low-energy polymorphs by force field

Table S10: Low-energy high-symmetry polymorphs by OPLS force field. Energy E_1 is in meV per monomer, distances are in Angstroms, a/c are polymer/ π -stacking translation periods, $a\Delta\xi/2$ is x -shift between adjacent polymer chains, q is the side-chain end-to-end vector. Alternative polymorphs of the same structural type and optimized experimental geometries are marked by prime. The π -stack from Ref.⁸ relaxes to *CAab* structure. The columns 100/200/300K show percentage of a dominant 2×2 structural pattern after melt-quench MD.

code	E_1	a	c	$\Delta\xi$	φ	δ	$q_{\bar{x}yqz}$	200 K	300 K	400 K
BDab	0	7.79	7.72	-0.41	16	111	245	100	100BDa	50BDaaaaaa
CBaac	8	7.74	7.80	-0.00	20	97	530	100	98CBa	100CBa
BDa	17	7.78	7.17	-0.28	7	90	344	92	54	58
ABAac	18	7.72	8.50	0.04	25	95	521	100	96BDa	77BDaaaaaa
CBab	28	7.75	8.13	0.19	21	118	045	97	100CBa	100CBa
CBabab	33	7.78	7.70	0.21	18	111	045	90	100CBa	96CBa
AAaac	41	7.80	8.60	0.00	34	87	521	98	68	B
DAaac	62	7.80	9.16	0.09	40	88	521	98	amorph	96Ca
CDab	66	7.82	7.87	0.23	16	119	135	CD/DBab	96Ca	95Ca
CAaac	67	7.80	7.64	0.12	17	90	531	100	98CBa	100CBa
CAabab	68	7.82	7.68	0.22	24	103	045	59	C	100Ca
BAab	72	7.83	7.56	-0.00	21	127	145	B	B	B
CAab	73	7.82	7.99	0.24	26	111	045	C	96Ca	100Ca
CDaac	78	7.78	7.96	-0.32	14	96	530	98Caac	C	88Ca
BDaac	80	7.75	8.19	-0.13	18	98	530			
BAaac	85	7.79	7.95	0.00	26	91	530			
BBab	85	7.83	7.80	0.00	16	122	135	100	96Ba	98Ba
BBAac	88	7.77	8.11	0.00	13	91	530			
BBa	92	7.81	7.15	0.00	8	91	154	61BBaa.aa	B	B
DDac	94	7.77	8.12	-0.46	15	95	136	100CBa	100CBa	93CBa
CBaab	100	7.72	7.70	-0.13	23	105	143			
DDaac	104	7.74	8.66	-0.30	20	96	531	100CBaacaa	100CBa	98CBa
Only unfolded conformers below this line										
BCa	114	7.84	7.20	0.00	4	87	254	B	95Ba	100Ba
BAa	115	7.79	7.24	-0.00	14	93	353			
CBa	126	7.72	7.75	-0.14	23	103	261	100CBa	100CBa	98CBa
AAa	179	7.80	8.67	0.00	34	85	351			
DBa	181	7.77	7.96	0.47	17	100	262			
CA ⁷	184	7.79	7.03	0.50	9	-164	163			
CBb	187	7.74	8.31	0.38	18	-145	045			
CCa	190	7.83	7.47	0.16	5	84	045			
CDa	190	7.83	7.69	0.06	4	86	154			
DA	191	7.79	9.50	-0.48	43	-176	145			
CAb	192	7.79	7.88	0.19	11	-103	045			
C	198	7.80	7.57	-0.38	0	180	160			
CAa	199	7.80	7.55	0.06	22	94	162	100Ca	96Ca	96Ca
DBa'	201	7.74	8.59	-0.27	20	94	352			
B	210	7.78	6.99	0.00	0	180	160			
CAa'	220	7.82	9.10	0.46	40	86	360			
Amorphous structures obtained by 1-400-400-1 K melt-quench with 1 ns per each step										
a-BDa	31	7.78	7.25	-0.29	8	90	343	from ABaac		
a-CBa	78	7.72	7.75	0	22	101	242	from CBaac		
a-Ca	86	7.66	7.80	0	± 20	± 102	140	from CAab		
a-Ba	86	7.70	7.42	0	± 9	± 95	240	from BCa		
π -stacks in bulk crystals										
CA ⁷	76	7.78	7.08	0.47	10	-167	162			
DA ⁷	—	7.7	7.6	-0.33	0	-150	154	C	C	89Ca
CAa ⁸	—	7.8	7.8	0.38	32	131	152			
i-DAA ⁶	—	7.77	9.44	0.08	43	97	160			
i-DAA	-138	7.81	8.67	0.33	36	98	061			
i-DAA'	-145	7.82	8.60	0.17	~ 35	~ 97	161	$\varphi = 34.3/35.5, \delta = 101/92$ (alternate)		

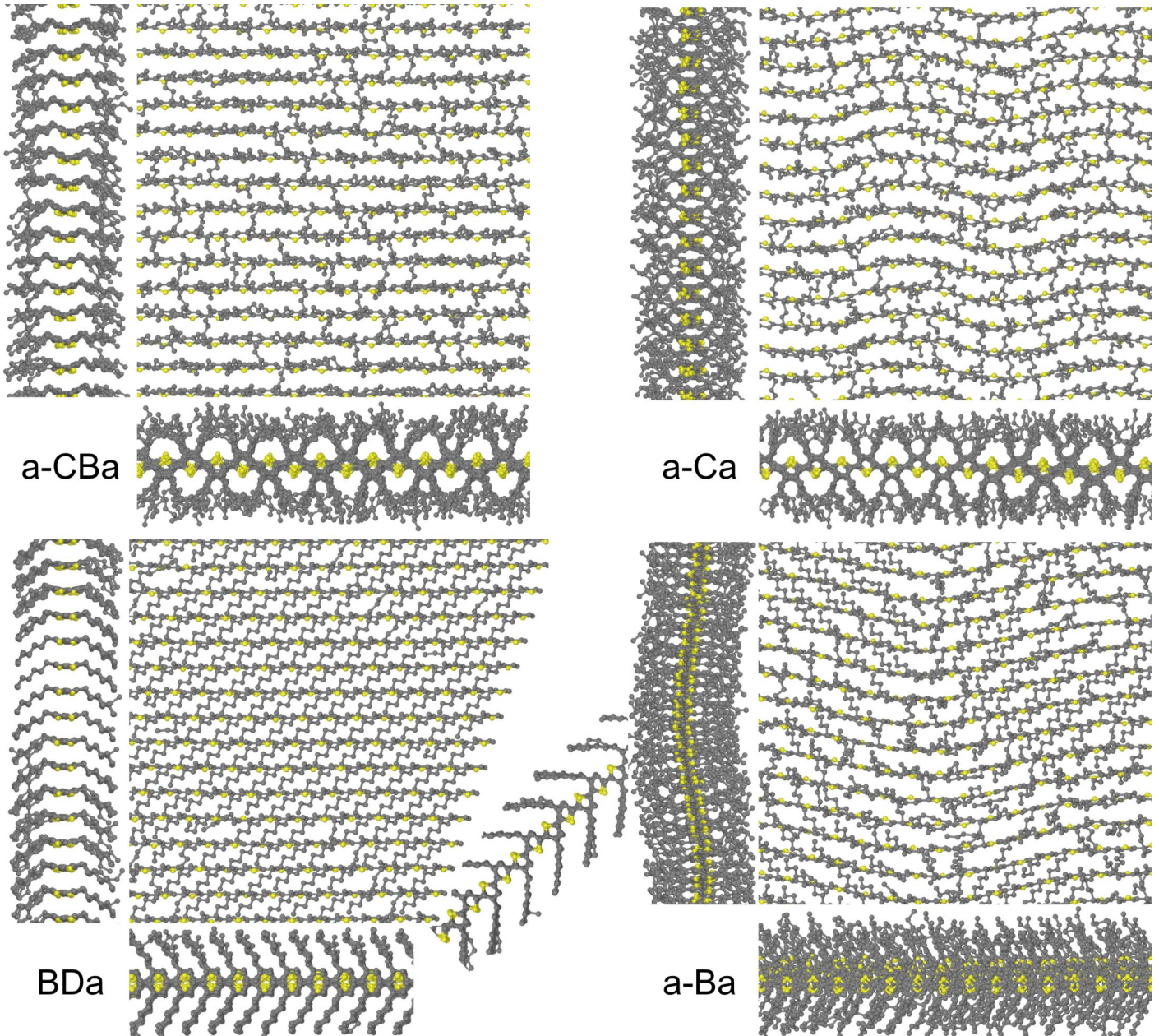


Figure S16: Four possible structures which can be obtained after MD melt-quench approach with temperature profile 1-400-400-1 K with 1 ns for each part. The supercell size is 16×16 monomers. The structure a-CBa is obtained from *CBaac* crystal, a-Ca is from *CAab*, and a-Ba is from *BCa*.

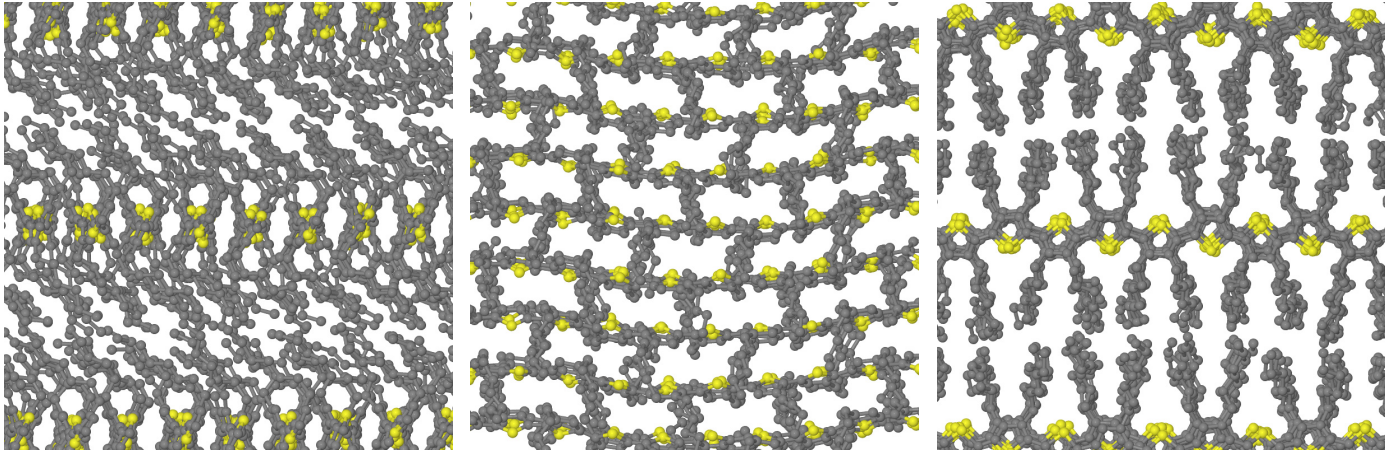


Figure S17: Crystal *Ca* from Ref.⁷ at 300 K: *x*, *y*, *z* projections.

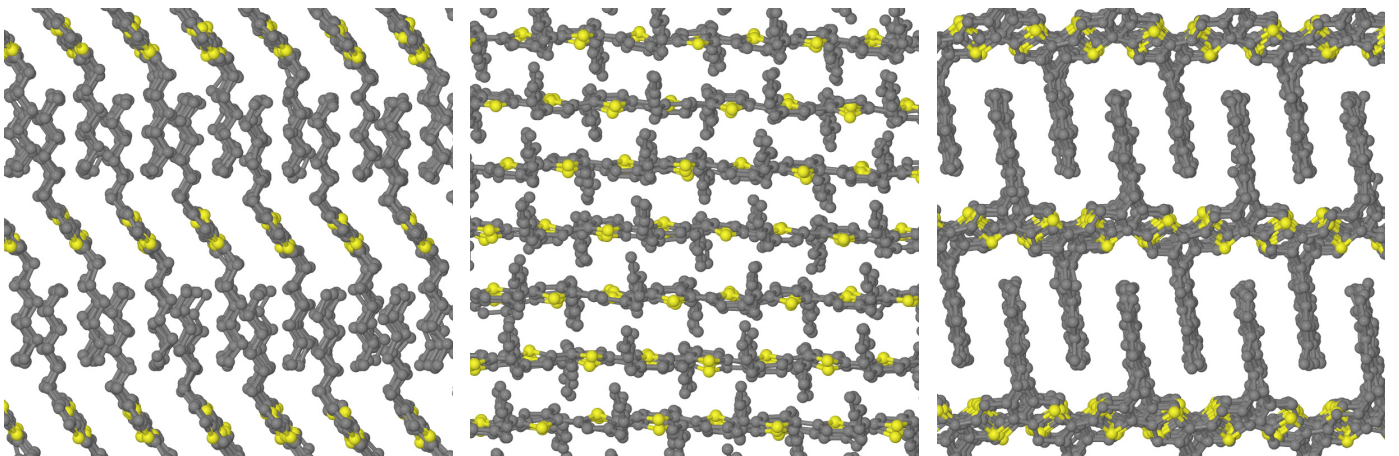


Figure S18: Fully interdigitated crystal i-DAa at 300 K: *x*, *y*, *z* projections.

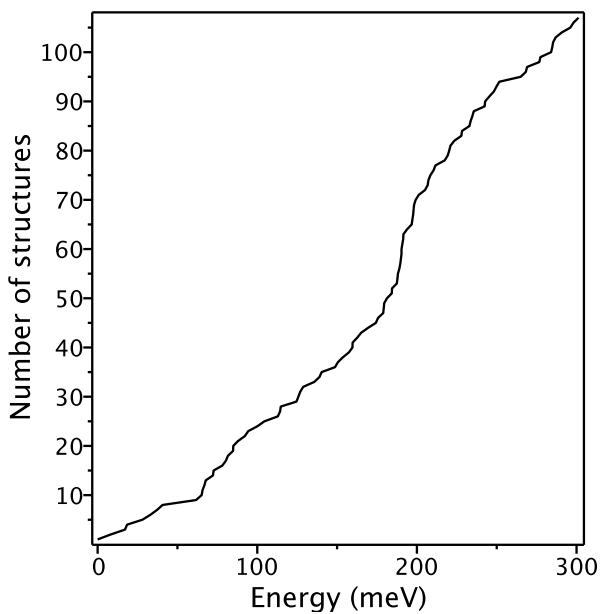


Figure S19: Distribution of structures by OPLS energy.

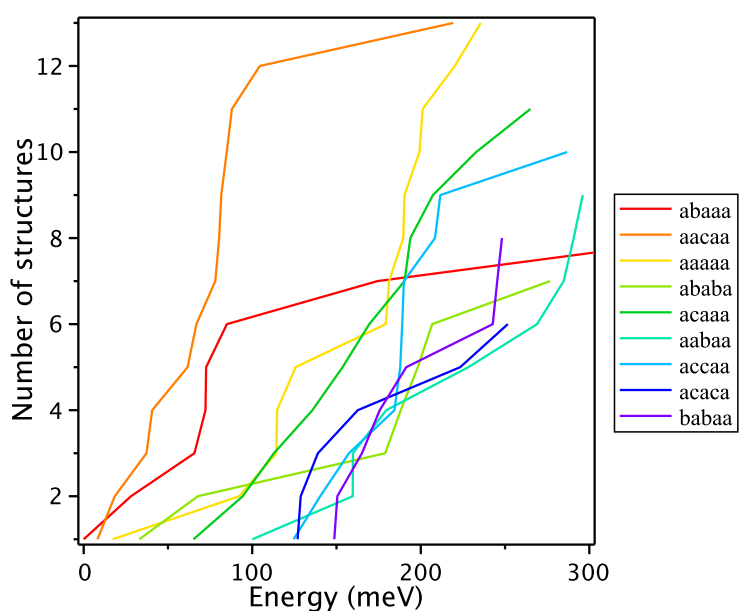


Figure S20: Distribution of structures by OPLS energy and side-chain conformation.

S8 Low-energy polymorphs by DFT

Table S11: List of low-energy high-symmetry polymorphs obtained by PBE-MBD method. See notations to Table S10.

code	E_1	a	c	$\Delta\xi$	φ	δ	$q_x q_y q_z$
CAaac	0	7.80	7.58	0.14	20	90	531
AAaac	9	7.78	8.63	0.00	35	87	52\bar{1}
CBaac	13	7.79	7.56	0.17	13	97	531
BAab	15	7.81	7.53	-0.00	21	129	\bar{1}45
CAab	17	7.81	7.87	0.23	25	113	045
DAAac	41	7.78	9.22	0.10	41	88	52\bar{2}
BAaac	44	7.79	7.90	0.00	25	91	530
BDA	45	7.79	7.31	-0.27	7	88	344
CAabab	45	7.81	7.54	0.22	23	104	045
BBAac	48	7.78	7.90	0.00	11	92	530
CBab	54	7.79	7.84	0.23	16	122	045
BDab	55	7.81	7.67	-0.41	12	114	235
Only selected conformers have been studied below this line							
BAacc	66	7.79	7.47	0.00	21	84	\bar{3}41
CBabab	69	7.79	7.45	0.23	15	113	045
BBa	79	7.80	7.29	0.00	9	90	154
BAa	87	7.79	7.37	-0.00	20	86	352
BCa	89	7.81	7.41	0.00	6	86	254
ABAac	94	7.77	8.42	0.04	23	99	52\bar{1}
C	95	7.79	7.40	-0.38	0	180	\bar{1}60
BAa'	111	7.79	7.38	0.00	2	99	244
CA'7	145	7.78	7.06	0.38	12	-168	\bar{1}63
CDa	159	7.82	7.73	0.06	4	84	154
CAa	159	7.80	7.50	0.06	24	93	162
CCa	160	7.82	7.42	0.21	7	85	045
CBb	160	7.80	7.60	0.38	12	-140	04\bar{5}
CAb	173	7.79	7.71	0.20	10	-106	04\bar{5}
B	187	7.77	7.05	0.00	0	180	\bar{1}60
AAa	196	7.80	8.93	0.00	37	83	351
CBa	197	7.78	7.55	-0.12	19	106	261
π -stacks in bulk crystals							
CA'7	29	7.79	7.13	0.41	9	-165	\bar{1}63
DA7	—	7.7	7.6	-0.33	0	-150	\bar{1}5\bar{4}
i-DAA ⁶	—	7.77	9.44	0.08	43	97	\bar{1}60
i-DAA	-128	7.80	8.88	0.26	38	95	061

Table S12: List of low-energy high-symmetry polymorphs obtained by vdW-DF2 method. See notations to Table S10. For the low-symmetry interdigitated structure i- DAa' the parameters are slightly modulated along the polymer: $\varphi = 38.0 \pm 0.16$, $\delta = 94.8 \pm 0.5$, $\delta_2 = 159.5 \pm 1.8$.

code	E_1	a	c	$\Delta\xi$	φ	δ	$q_x q_y q_z$
CAaac	0	7.87	7.81	0.14	20	89	531
CBAac	16	7.86	7.84	0.12	15	98	531
CAab	19	7.89	8.00	0.24	25	114	045
AAaac	23	7.87	8.95	0.00	36	88	521
BAab	34	7.89	7.72	0.00	20	129	145
BAAac	35	7.87	8.00	-0.00	24	91	530
BBAac	36	7.86	8.04	0.00	11	92	530
BDA	40	7.87	7.46	-0.25	6	89	344
CBab	50	7.88	7.99	0.24	16	122	045
CAabab	57	7.89	7.77	0.24	23	105	045
BDab	60	7.88	7.93	-0.40	13	114	245
CDAac	60	7.87	7.98	-0.17	10	99	530
Only selected conformers have been studied below this line							
BAac	68	7.88	7.57	0.00	16	82	145
CAaacac	70	7.92	7.95	0.34	22	89	045
BAacc	80	7.87	7.57	-0.00	19	84	341
BAa	87	7.87	7.51	0.00	18	87	353
BBA	96	7.89	7.52	0.00	9	89	254
BAa'	97	7.87	7.48	-0.00	8	96	254
ABAac	101	7.85	8.75	0.05	24	98	531
BCa	114	7.91	7.57	-0.00	6	85	254
CAb	163	7.88	7.48	0.29	3	-108	045
C	165	7.87	7.62	-0.38	0	180	160
CAa	166	7.88	7.45	0.18	17	94	162
CA ⁷	196	7.87	7.39	0.40	13	-164	154
CBa	216	7.85	7.75	-0.11	19	104	261
B	229	7.84	7.06	0.00	0	180	160
AAa	231	7.88	9.07	0.00	36	83	451
π -stacks in bulk crystals							
CA ⁷	42	7.86	7.41	0.43	13	-162	154
DA ⁷	—	7.7	7.6	-0.33	0	-150	154
i-DAa ⁶	—	7.77	9.44	0.08	43	97	160
i-DAa	-148	7.89	9.07	0.26	38	94	061
i-DAa'	-148	7.89	9.06	0.29	~38	~95	061

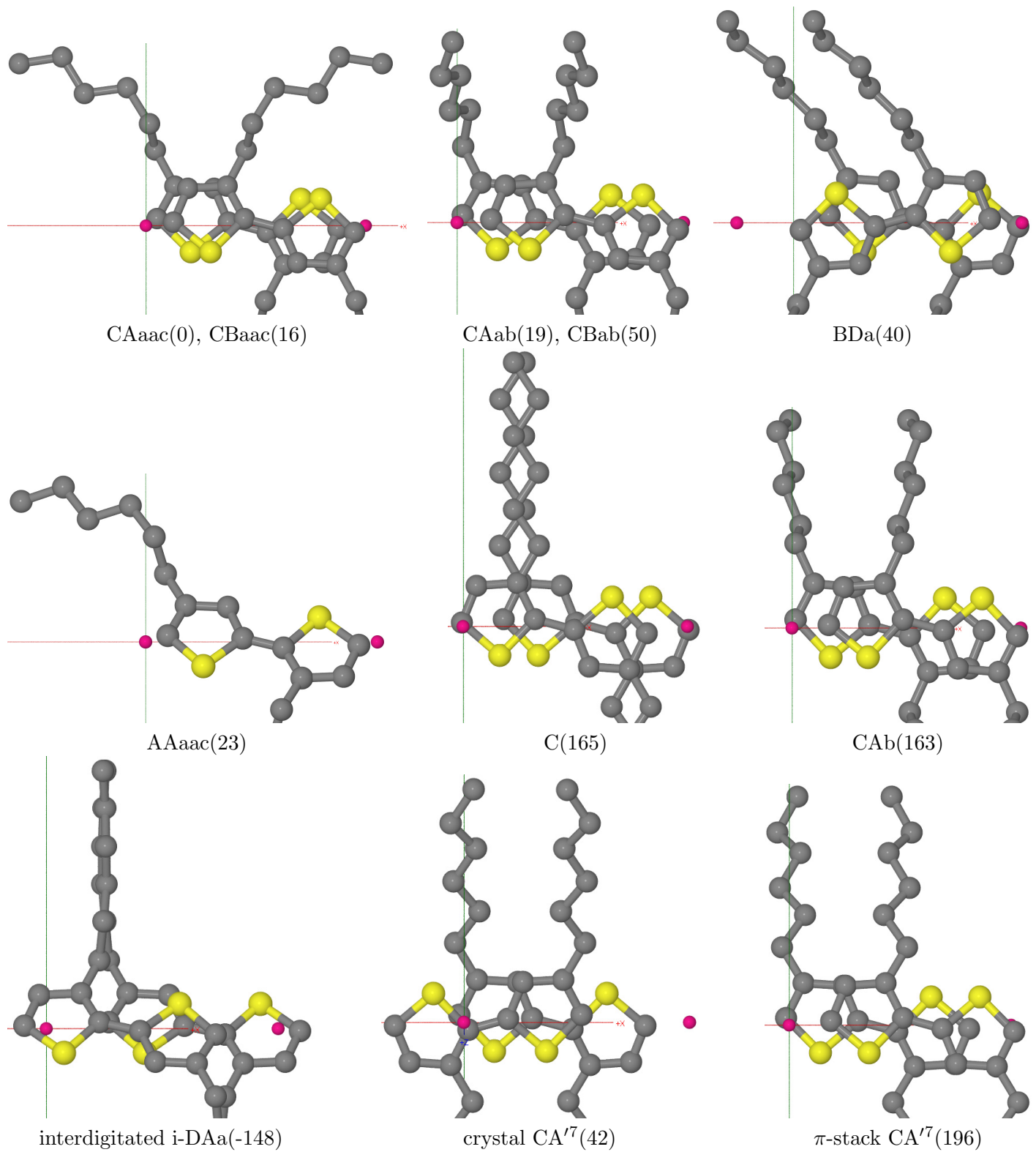


Figure S21: Unit cell of selected polymorphs viewed along z -axis. The vdW-DF2 energies in meV are given in parentheses. Unit cells are denoted by translation vectors starting at the origin and ending at magenta balls. The x - and y -axes are marked by red and green colors respectively. Structural types *CA* and *CB* have nearly the same z -projection.

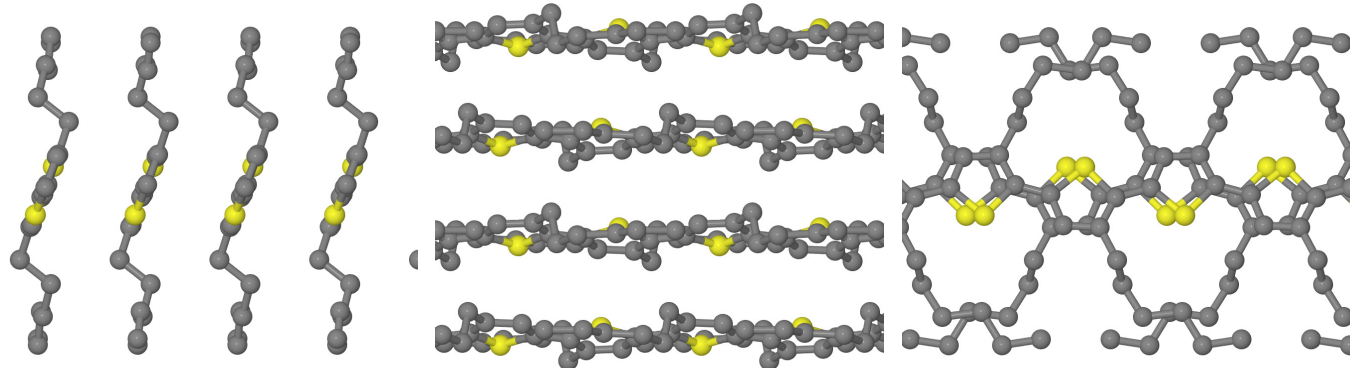


Figure S22: π -stack CAaac: x , y , z projections.

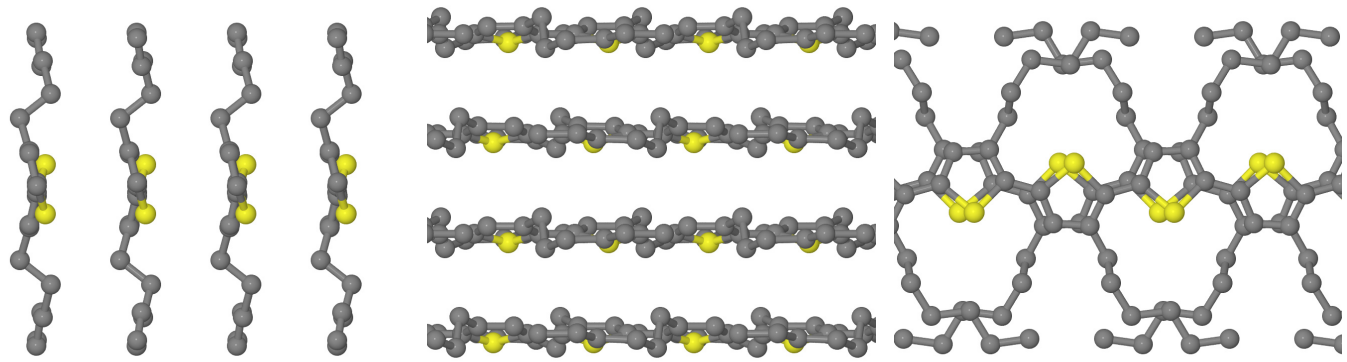


Figure S23: π -stack CBaac: x , y , z projections.

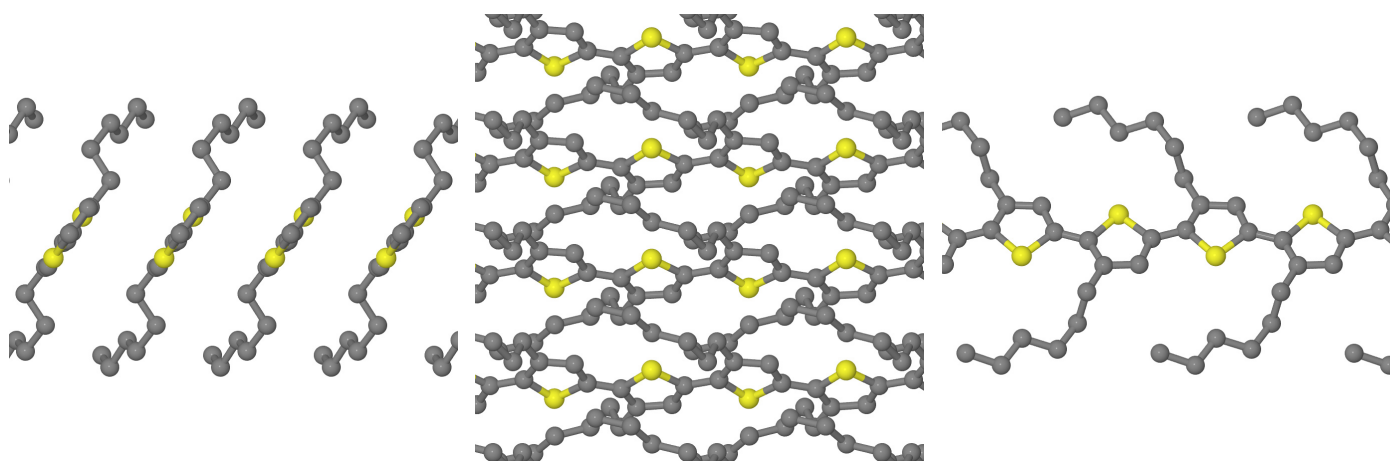


Figure S24: π -stack AAaac: x , y , z projections.

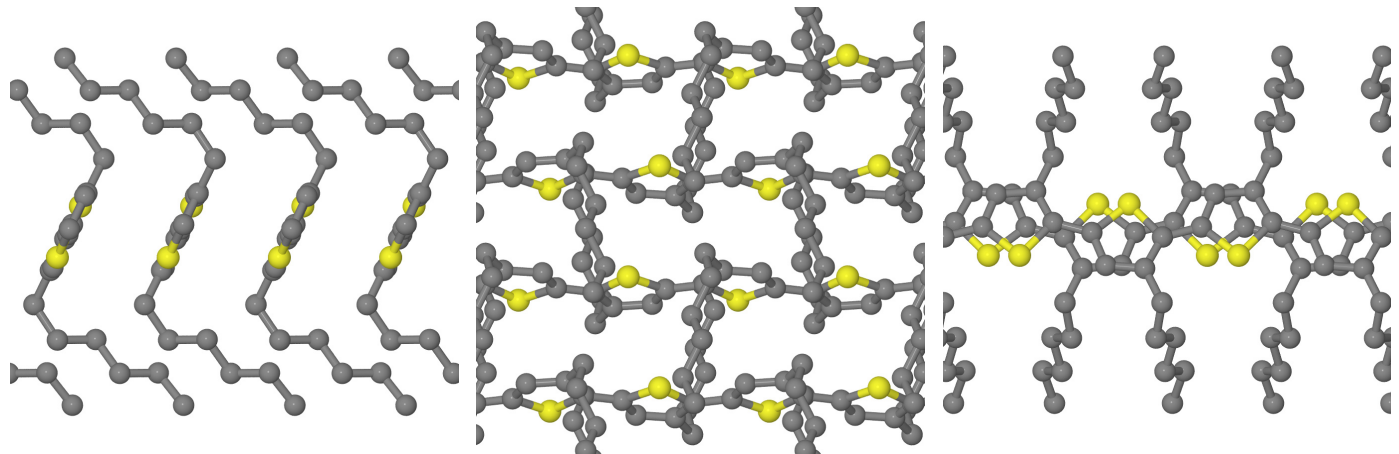


Figure S25: π -stack *CAab*: x , y , z projections.

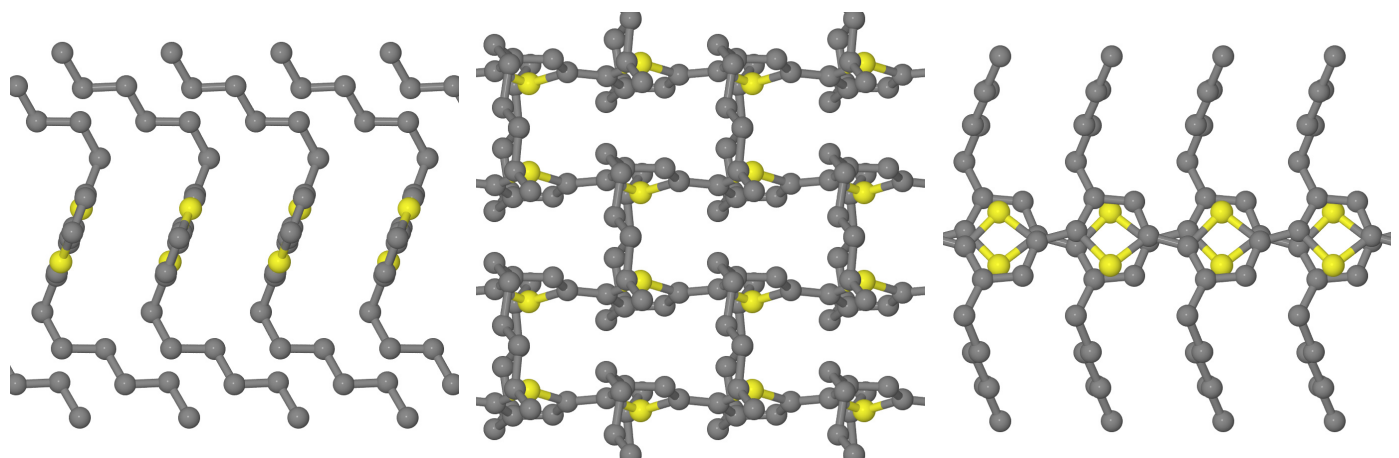


Figure S26: π -stack *BAab*: x , y , z projections.

Table S13: Relative energies (in meV) of different polymorphs by different methods with geometries relaxed by the OPLS force field. The CAM-B3LYP-D3 value is estimated by formula Eq. (S2).

code	PBE-MBD	vdW-DF2	CAM-B3LYP-D3	OPLS
AAaac	0	25	0	41
CAaac	7	0	28	67
BAab	21	23	28	72
CAab	22	11	16	73
DAaac	34	56	78	62
CBaac	40	29	24	8
BAaac	42	30	42	85
CAaabab	42	51	26	68
BBAac	48	25	53	88
BDa	51	51	31	17
BDab	63	71	43	0
BAacc	68	68	60	125
CBbabab	70	71	40	33
BBa	71	83	48	92
CBab	72	61	42	28
CAaacac	79	65	80	139
BBab	79	79	61	85
CDab	80	92	77	66
CDAac	80	65	99	78
BAac	88	63	76	113
BCa	88	102	85	114
BAa	94	76	76	116
ABAac	96	109	66	18
BAaab	103	82	86	160
C	105	144	163	198
Only unfolded conformers below this line				
BAb	118	97	126	147
CA'7	144	167	151	184
CAa	154	165	155	200
CDa	155	161	179	190
CCa	163	156	188	194
CAb	170	175	195	192
B	185	206	189	210
AAa	189	232	214	179
CBb	192	193	205	187
DAa	199	223	226	221
CBa	199	212	167	126
BDb	212	219	261	242
DBa	219	226	270	181

Bulk P3HT energy for CAM-B3LYP-D3 method in Table S13 is roughly estimated within cluster approach by the following formula:

$$E = E_{22} - E_{21} - E_{12} + E_{11}, \quad (\text{S2})$$

where E_{mn} is the energy of the hydrogen-passivated $m \times n$ supercell. This formula is exact for a rectangular lattice with nearest neighbor interactions. Indeed, if we write the bulk energy as $E = E_0 + V_1 + V_2$, where E_0 is some “internal” energy of the unit cell and $V_{1,2}$ are the cell-cell interaction energies along each direction then

$$E_{mn} = mnE_0 + (m-1)nV_1 + m(n-1)V_2 + n\varepsilon_1 + m\varepsilon_2 \equiv mnE + n(\varepsilon_1 - V_1) + m(\varepsilon_2 - V_2), \quad (\text{S3})$$

where $\varepsilon_{1,2}$ are the total (both sides) hydrogen passivation energies along each direction. More accurate estimates are possible with more deliberate selection of clusters, but that requires substantial computational efforts beyond the scope of the present work.

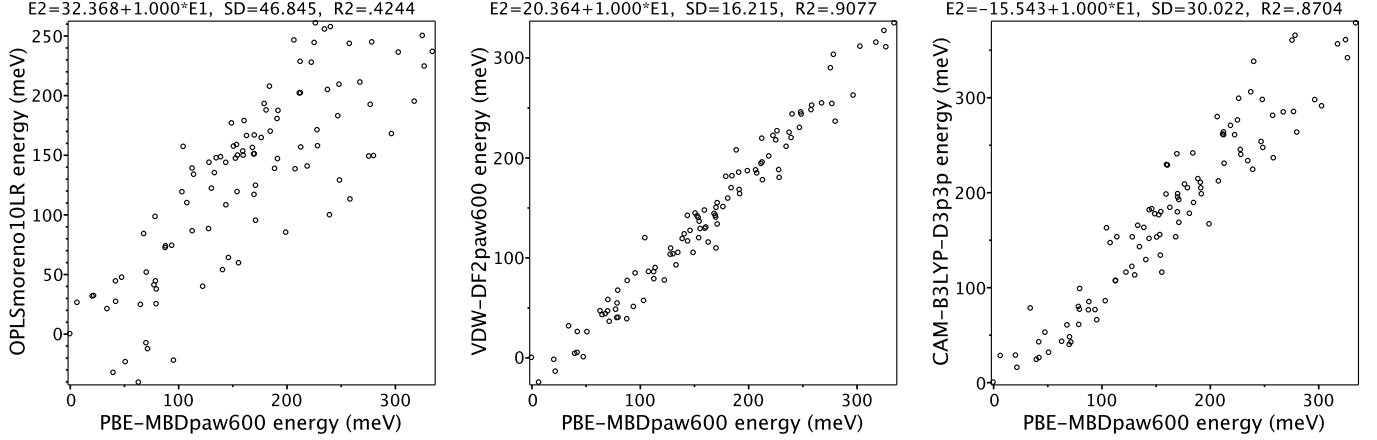


Figure S27: Accuracy of different methods compared to PBE-MBD for all low-energy π -stacks generated by OPLS force field.

S9 Elastic constants and vibrational frequencies

Table S14: Lowest vibrational frequencies at Γ -point by vdW-DF2. Negative values mean imaginary frequencies.

code	E_1 (meV)	frequencies (meV)									
		2.63	3.83	4.42	4.81	5.24	5.39	6.51	6.86	7.85	7.90
CAaac	0	2.63	3.83	4.42	4.81	5.24	5.39	6.51	6.86	7.85	7.90
CBaac	15	2.48	2.71	3.58	4.55	4.68	5.11	6.24	6.30	8.43	8.46
CAab	19	4.12	4.19	4.80	5.04	5.14	5.93	6.94	6.98	7.43	7.89
AAaac	23	3.28	3.42	4.09	4.94	6.64	7.06	7.20	7.42	7.86	8.26
BAab	34	3.66	3.91	4.72	5.09	5.84	6.18	6.85	6.87	7.62	7.90
BAaac	35	2.11	3.14	4.29	4.30	5.73	6.09	6.49	6.53	7.79	8.04
BBAac	36	0.42	1.48	2.50	3.48	4.74	4.74	5.81	6.25	6.65	6.67
BDA	41	2.58	3.53	3.93	4.22	4.76	6.90	7.38	7.58	7.69	7.89
CBab	50	3.72	3.85	4.43	5.05	5.27	6.71	7.00	7.13	7.46	7.70
CAabab	57	4.25	4.31	5.41	5.61	5.92	6.21	7.44	7.84	8.24	8.28
BDab	60	3.06	4.00	4.02	5.36	5.49	7.23	7.76	7.92	7.99	8.88
CDAac	60	-1.74	2.63	2.87	3.54	5.00	5.41	5.93	5.96	7.22	8.11
BAac	69	2.69	2.87	3.07	3.44	3.92	5.21	5.71	5.94	6.40	6.65
CAacac	70	3.12	3.89	4.01	4.81	5.08	6.04	6.48	6.75	6.84	6.88
BAacc	80	3.24	3.62	3.74	4.15	4.96	5.33	5.98	6.26	6.49	7.12
BAa	88	2.28	2.28	2.32	2.35	3.10	3.67	3.79	4.10	5.99	6.04
BBa	96	0.62	2.60	2.66	3.14	3.59	3.72	4.01	4.71	6.56	7.80
BAa'	97	1.99	2.00	2.23	2.37	3.88	3.89	3.93	3.94	5.41	5.92
CAb	163	1.05	2.37	2.62	3.04	3.38	4.16	4.28	4.54	4.57	5.21
C	164	0.71	2.33	2.73	2.99	3.52	4.47	5.10	5.61	5.78	7.26
CAa	166	1.31	1.96	2.21	2.73	4.15	4.35	5.56	5.58	5.64	5.87
CA'7	196	0.47	0.88	1.65	2.35	2.67	2.79	4.11	4.24	4.39	4.96
CBa	215	1.85	2.20	2.32	2.69	3.64	4.08	4.25	4.56	5.17	5.23
bulk crystals											
CA'7	42	-1.13	2.68	3.11	4.33	4.65	4.70	6.20	6.63	7.72	8.72
i-DAA	-148		3.50	5.05	5.29	5.48	6.39	7.16	7.85	8.13	8.20
											9.29

Table S15: Eigenvalues of the two-dimensional elasticity tensor by vdW-DF2. The dominant projections of each eigenvalue are the same for all structures and are given in the second row. For three-dimensional crystal $CA'7$ the eigenvalues (in GPa) are 0.40, 4.82, 23.60 mostly in subspace $YY + ZZ + YZ$, 1.34 (XZ), 6.60 (XY), 127.03 (XX). For i-DAa the eigenvalues are -0.83 and 1.31 in $XY + XZ$, 4.47 (YZ), 9.46 and 25.71 in $YY + ZZ$, 141.74 (XX).

code	E_1 (meV)	eigenvalues (GPa)		
		XZ	ZZ	XX
CAaac	0	0.70	7.25	68.64
CBaac	15	0.74	6.43	64.87
CAab	19	0.54	4.75	65.76
AAaac	23	0.89	3.04	60.87
BDA	41	1.04	5.87	70.11
CAb	162	-1.06	2.39	67.16
C	162	0.32	8.88	68.39
CA'7	196	-0.09	1.54	66.95

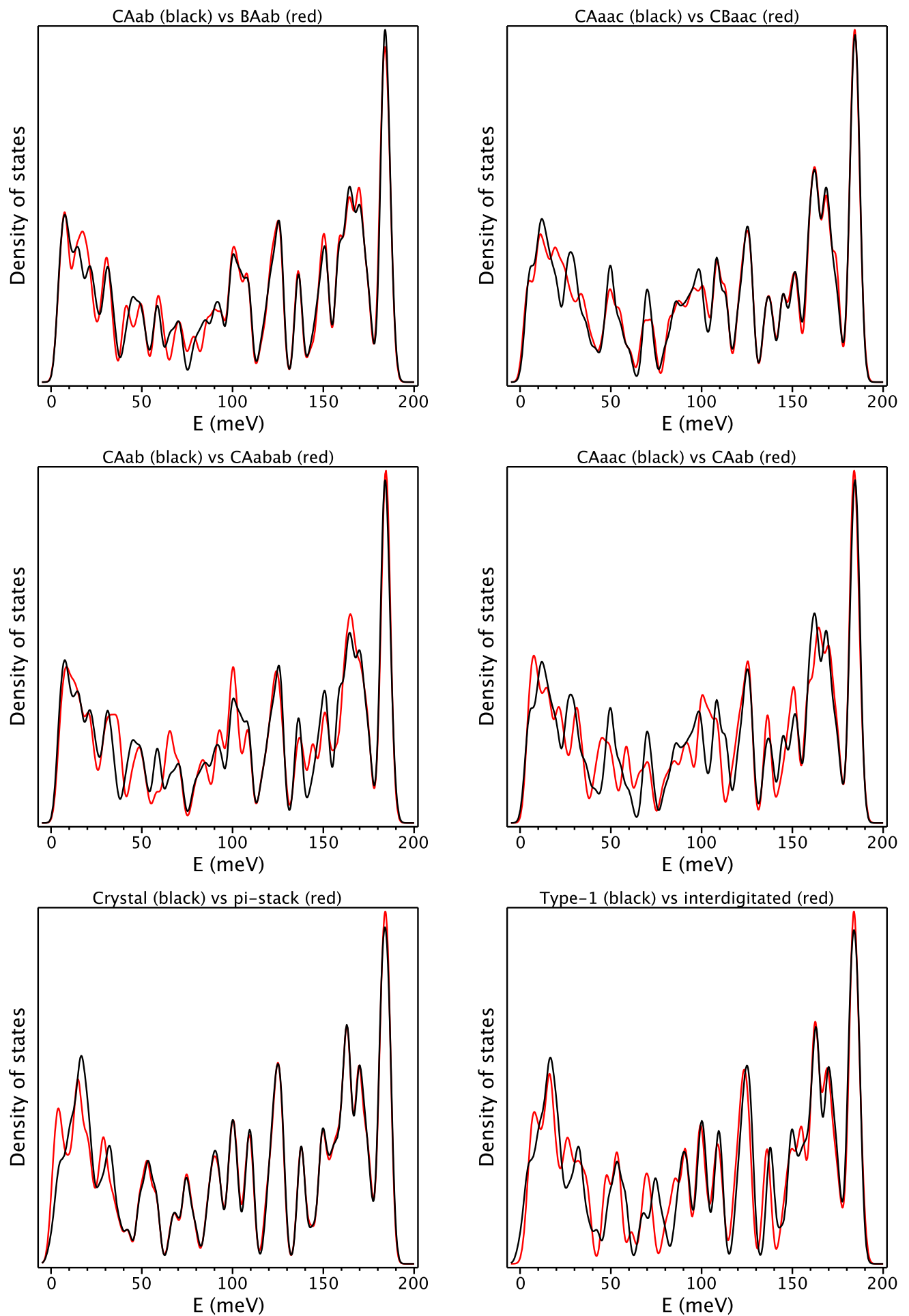


Figure S28: Vibrational DOS for various polymorphs in pairwise comparison.

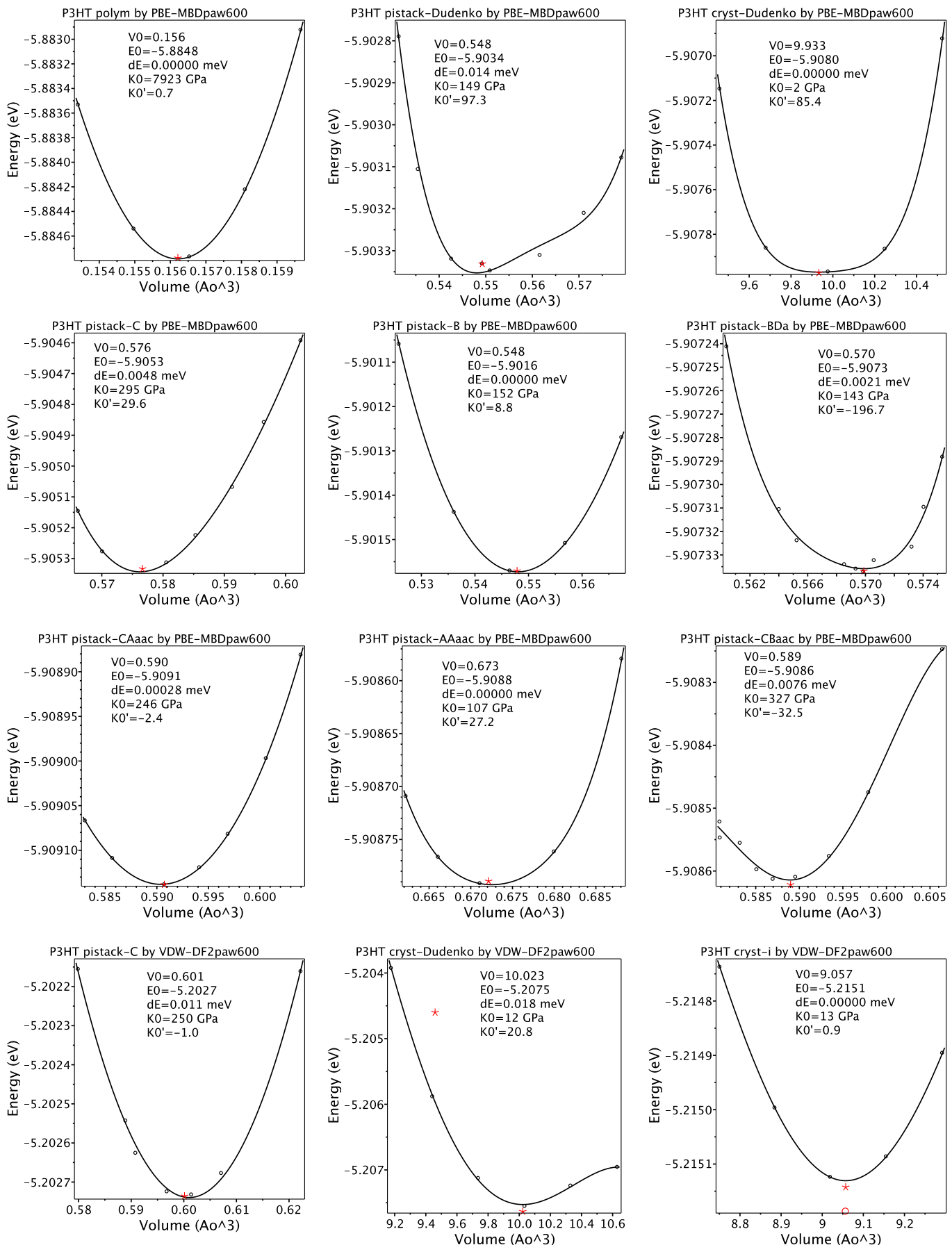


Figure S29: Equation of state derived from geometry optimization for selected polymorphs.

S10 Electronic structure

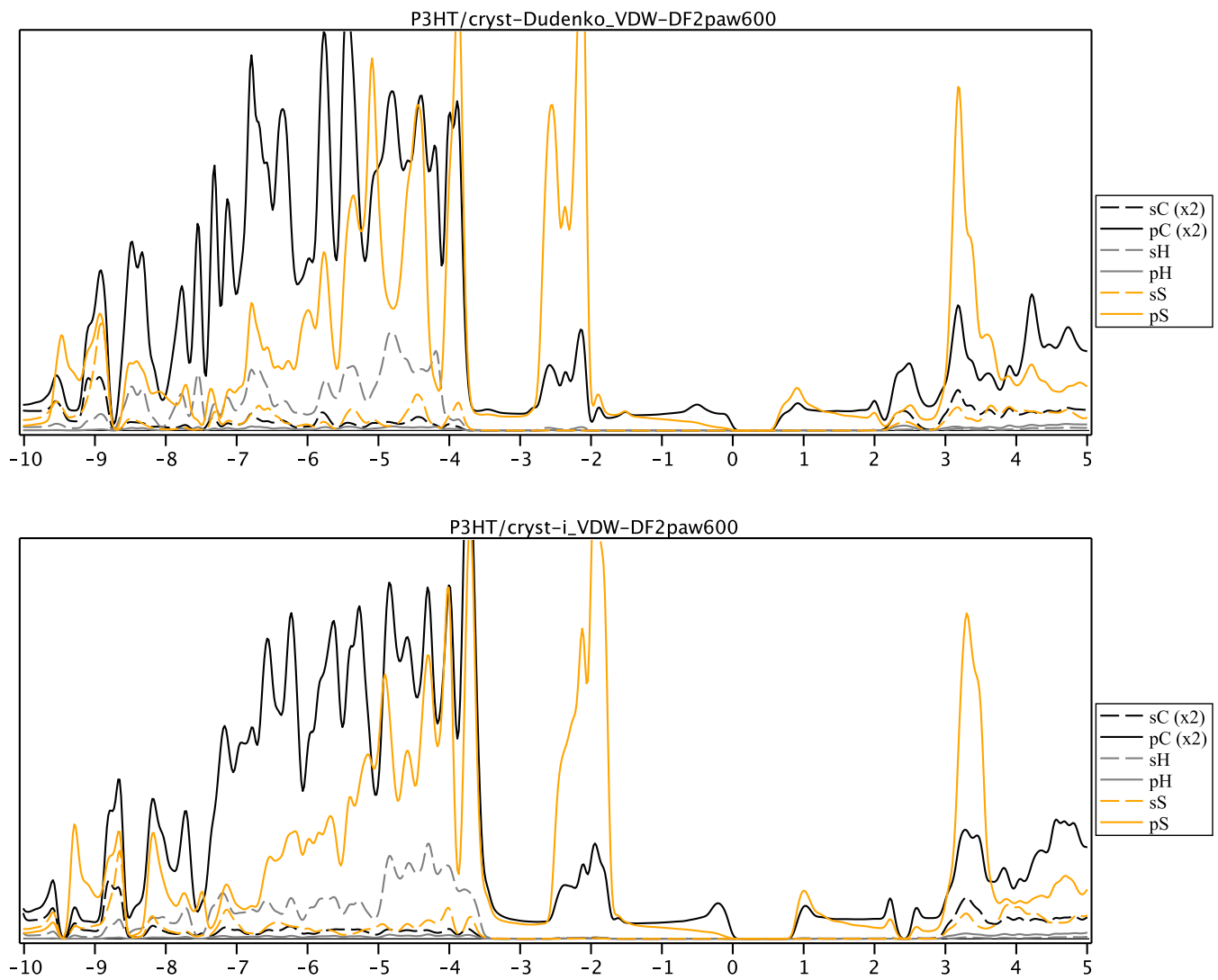


Figure S30: Electronic density of states for bulk crystals.

S11 Selected tables recalculated in kcal/mol energy unit

Table S16: Table 2 from the main text in kcal/mol units.

	PE	PT	M
dataset size	6	7	72
6-311G*			
CAM-B3LYP-D3	0.115	0.208	0.115
B3LYP-D3	0.369	0.115	0.277
PBE-MBD	0.507	0.530	0.300
vdW-DF2	0.438	0.461	0.392
LC- ω PBE-D3	1.153	0.346	0.553
ω B97XD	2.075	0.369	0.600
OPLS	2.721	1.245	1.291
CAM-B3LYP	4.497	0.208	1.476
CAM-B3LYP-D3			
6-311G*	0.115	0.208	0.115
6-311G**	0.184	0.184	0.138
6-311+G(3df,2p)	0.231	0.023	0.277
6-31G*	0.438	0.138	0.138

References

- [1] Jones, M. L.; Huang, D. M.; Chakrabarti, B.; Groves, C. Relating Molecular Morphology to Charge Mobility in Semicrystalline Conjugated Polymers. *J. Phys. Chem. C* **2016**, *120*, 4240-4250.
- [2] Byrd, J. N.; Bartlett, R. G.; Montgomery, J. A. At What Chain Length Do Unbranched Alkanes Prefer Folded Conformations? *J. Phys. Chem. A* **2014**, *118*, 1706-1712.
- [3] Samdal, S.; Samuelsen, E. J.; Volden, H. V. Molecular Conformation of 2,2'-Bithiophene Determined by Gas Phase Electron Diffraction and Ab Initio Calculations. *Synth. Met.* **1993**, *59*, 259-265.
- [4] Busing, W. R. X-ray Diffraction Study of Disorder in Allied Spectra-1000 Polyethylene Fibers. *Macromolecules* **1990**, *23*, 4608-4610.
- [5] Siegrist, T.; Kloc, C.; Laudise, R. A.; Katz, H. E.; Haddon, R. C. Crystal Growth, Structure, and Electronic Band Structure of a-4T Polymorphs. *Adv. Mater.* **1998**, *10*, 379-382.
- [6] Rahimi, K.; Botiz, I.; Stingelin, N.; Kayunkid, N.; Sommer, M.; Koch, F. P. V.; Nguyen, H.; Coulembier, O.; Dubois, P.; Brinkmann, M. et al. Controllable Processes for Generating Large Single Crystals of Poly(3-hexylthiophene). *Angew. Chem. Int. Ed. Engl.* **2012**, *51*, 11131-11135.
- [7] Dudenko, D.; Kiersnowski, A.; Shu, J.; Pisula, W.; Sebastiani, D.; Spiess, H. W.; Hansen, M. R. A Strategy for Revealing the Packing in Semicrystalline pi-Conjugated Polymers: Crystal Structure of Bulk Poly(3-hexyl-thiophene) (P3HT). *Angew. Chem. Int. Ed. Engl.* **2012**, *51*, 11068-11072.
- [8] Kayunkid, N.; Uttiya, S.; Brinkmann, M. Structural Model of Regioregular Poly(3-hexylthiophene) Obtained by Electron Diffraction Analysis. *Macromolecules* **2010**, *43*, 4961-4967.